Diagnoses of an Eddy-Resolving Atlantic Ocean Model Simulation in the Vicinity of the Gulf Stream. Part I: Potential Vorticity

MOTOTAKA NAKAMURA AND YI CHAO

Jet Propulsion Laboratory, California Institute of Technology, Pasadena, California

(Manuscript received 7 January 1999, in final form 14 March 2000)

ABSTRACT

Output of an eddy-resolving model of the North Atlantic is diagnosed in the vicinity of the Gulf Stream (GS), using quasigeostrophic potential vorticity (QGPV), Ertel's potential vorticity (PV), and particle trajectories. Time series of QGPV show strong input of QGPV by the GS in the top 1000 m of the model ocean. Vigorous wave motions are observed in the vicinity of the model GS, mixing QGPV in the region. The time-mean horizontal QGPV structures show qualitative similarity to those of large-scale climatological PV calculated from hydrographic data by Keffer and that of Lozier. The top 1000 m of the model ocean is characterized by a tongue or an elongated island of high mean QGPV along the GS. It is demonstrated that the tongue is a product of strong QGPV input by the GS, vigorous mixing by eddies, and dissipation of QGPV along the path of the GS. At the intermediate depths, 1000–2500 m, a large region of nearly homogenized mean PV or weakly varying mean QGPV is found to the west of the Mid-Atlantic Ridge. It is located undernearth a region of strong near-surface eddy activity and is in qualitative agreement with a deep and large pool of nearly homogenized PV recently found by Lozier. Below the pool of nearly homogenized PV or weakly varying QGPV, the mean PV and QGPV show substantial horizontal gradient and some vertical gradient at deep levels. This structure is in qualitative agreement with results of idealized model experiments and a theory of baroclinic neutrality of the midlatitude atmosphere proposed by Lindzen that may well apply to this oceanic region of strong baroclinic wave activity.

1. Introduction

It has become increasingly clear that the atmosphere and oceans interact with each other on regional and global scales and produce variability of various kinds in the global and regional climates. Aside from the well-known El Niño phenomenon, there are pieces of evidence that the North Atlantic and the North Pacific interact with the atmosphere in complex ways and generate variabilities of various timescales in oceanic and atmospheric states (e.g., Palmer and Sun 1985; Wallace et al. 1990; Cayan 1992a,b; Ferranti et al. 1994; Hurrell and Van loon 1997). Sharp oceanic fronts associated with the Gulf Stream (GS) and the Kuroshio Current are known to be important forcing factors for the midlatitude atmosphere (e.g., Hoskins and Valdes 1990; Ferranti et al. 1994) and their variabilities are bound to be accompanied by variabilities in the midlatitude atmosphere. While being important factors to midlatitude atmospheric forcing, the oceanic fronts are also forced by the atmosphere, suggesting a mutually sustaining relationship between the oceanic fronts and the midlatitude atmosphere. The oceanic fronts affect not only the near-surface circulations and fluxes of heat and salt, but also those at depth, as shown here and in a separate paper, possibly modulating the thermohaline circulation through their influence on the deep circulations. It is, thus, crucial to understand the dynamics of these oceanic fronts in order to understand the role of oceans and interactions between the atomsphere and oceans in regional and global climates and their fluctuations.

Analyses of large-scale oceanic circulations have been limited due to the difficulty in collecting observational data at sufficiently high resolution in space and time over an extended period and area. In the absence of sufficient oceanic data to analyze the entire region surrounding the oceanic fronts, utilizing output of eddy-resolving models for studying the fronts seems to be a rational approach. Needless to say, the models are far from perfect and their solutions have unrealistic features. Nonetheless, diagnoses of model output in a framework based on dynamical ideas may be useful in learning, at least qualitatively, the dynamics of the circulations in the vicinity of the fronts and also in deducing the causes of unrealistic features in the model, providing potentially useful information for future improvements in models. Such diagnoses may also provide us with helpful information for guiding observational efforts.

Corresponding author address: Dr. Mototaka Nakamura, Jet Propulsion Laboratory, California Institute of Technology, Mail Stop 300-323, 4800 Oak Grove Drive, Pasadena, CA 91109.
E-mail: moto@pacific.jpl.nasa.gov

© 2001 American Meteorological Society

The central quantity in studies of large-scale dynamics of the atmosphere and oceans is potential vorticity (PV). Frameworks based on PV have been used widely for theories of large-scale circulations in the atmosphere and oceans and has provided useful insight into the dynamics of the large-scale circulations. Two examples of such theories are Eady's stability theory for baroclinic flows (Eady 1949) and the theory for the wind-driven ocean circulation postulated by Rhines and Young (1982a,b). In studies of the atmospheric circulations, for which sufficient observational data have been available, PV has also been used widely for diagnostics (e.g., Illari and Marshall 1983; Hoskins and Sardeshmukh 1987). An approximate form of PV, quasigeostrophic PV (QGPV), also has been used as a framework in building numerical models of the midlatitude atmosphere and oceans (e.g., Phillips 1954; Holland 1978). A property of PV that makes it so useful in studying large-scale circulations is the conservation of PV in the absence of heating/cooling and friction following a parcel. For studying the oceanic flows, this property is particularly useful since oceanic water moves primarily along isopycnal surfaces in the interior; thus, theories for distribution of PV and potential density are essentially theories for the circulation. This is reflected in the invertibility principle that states that one can obtain the circulation field, given the distribution of PV, boundary conditions, and an assumption of a certain balance condition, such as quasigeostrophy (Hoskins et al. 1985).

While diagnoses of the atmospheric circulations with PV have been common in the past, diagnostic attempts on oceanic flows have been very limited due to the lack of data. However, some calculations of PV for the climatological state of the ocean have been made by several investigators. The pioneering work was done by Behringer (1972), who produced maps of PV for two isopycnal intervals for the South Atlantic, using data from the *Meteor* expedition. Following Behringer, McDowell et al. (1982) computed PV for the North Atlantic for five isopycnal intervals, using hydrographic data from the 1957–58 IGY program and the *Erika Dan* sections of 1962. Maps of PV for the global oceans were produced by Keffer (1985) from the climatological atlas of Levitus (1982) for four layers. Recently, Lozier (1997) calculated PV for deeper parts of the North Atlantic, using an improved hydrographic dataset (Lozier et al. 1995). The maps of PV produced by these investigators have provided us with useful insight into the mechanisms of large-scale oceanic circulations at various depths with the aid of circulation theories and idealized models based on QGPV (Rhines and Holland 1979; Holland and Rhines 1980; Rhines and Young 1982a,b). [See Holland et al. (1984) for a review of the theory and discussion on observed PV fields.] Despite the usefulness of the maps of PV produced from the climatological data, they show only large-scale quasi-steady states and lack the information on the role of eddies (perturbations from the climatological state) in the dynamics of the large-scale circulation.

Attempts to understand large-scale ocean circulations with the presence of eddies, using PV or QGPV, have been made in the past with eddy-resolving general circulation models (GCMs) in idealized geometries. Holland and Rhines (1980) were the first to analyze large-scale circulations in a framework of QGPV, eddy enstrophy, and eddy QGPV fluxes, using an idealized quasigeostrophic eddy-resolving model of a wind-driven circulation. One of the most important findings in their study, to be confirmed by subsequent studies by others (e.g., Holland et al. 1984; Cox 1985; Lozier and Riser 1989, 1990), is the generation of a large region of nearly homogenized QGPV in midlayers by the action of eddies, although there are differences in details among the models used by these investigators. Holland and Rhines (1980) suggest that enstrophy cascade plays an important role in driving the mean circulation. Lozier and Riser (1989, 1990) used a model similar to that used by Holland and Rhines (1980) to study source and sink of QGPV in an idealized ocean. Rhines and Schopps (1991) also used an idealized eddy-resolving model based on QGPV and reported strong eddy mixing and QGPV homogenization in the gyre interior. They note fairly small Peclet number in the midlayers in general, consistent with the strong eddy mixing found in the interior ocean. While most of these studies were done with a quasigeostrophic model, using QGPV as a key quantity of analyses, Cox (1985) used a primitive equation GCM, driven by an idealized wind stress pattern and bouyancy forcing, to study large-scale circulations in an idealized North Atlantic ocean. Despite differences in the structure, Cox (1985) also found a large region of nearly homogenized PV in the gyre interior in the thermocline. He notes that rapid mixing may homogenize PV even when the isopycnal layer is ventilated. Spall (1996) used an isopycnal coordinate model of an idealized North Atlantic to study the GS/deep western boundary current (DWBC) crossover dynamics and found PV to be nearly homogenized under the GS where eddy mixing is strong.

Here, we attempt to study quasi-horizontal large-scale circulations in the vicinity of the GS in a framework based on QGPV, using a 5-yr output of an eddy-resolving ocean GCM of the North Atlantic that has realistic surface forcings and bottom topography. This study may be thought of as an extension of past works by other investigators mentioned above to a more realistic ocean flow. We focus our attention on interpretation of the mean field in this paper, while eddy enstrophy and eddy fluxes are treated in a separate paper (Nakamura and Chao 2000a, manuscript submitted to *J. Phys. Oceanogr.,* hereafter NC). The main purpose of the study is to examine the mechanisms that are responsible for the large-scale low-frequency QGPV structures and the low-frequency flows in the vicinity of the GS, using the model output as pseudodata. Section 2 briefly describes

the model output used for the diagnostics. Section 3 describes the calculation procedure of PV. Section 4 describes and discusses the results of the calculations. Finally, section 5 summarizes the results.

2. Pseudodata

The pseudodata used for the calculations are from a 30-yr integration of an eddy-resolving general circulation model of the North Atlantic described by Chao et al. (1996). The model is based on the Parallel Ocean Program (POP) developed at Los Alamos National Laboratory (Dukowicz and Smith 1994). The POP is a free-surface version of the primitive-equation model developed at the Geophysical Fluid Dynamics Laboratory (Bryan 1969; Cox 1984). The model basin covers the Atlantic basin from 35°S to 80°N, 100°W to 20°E. The horizontal grid spacing of the model is approximately $\frac{1}{6}$° (0.1843° lat by 0.1875° long). There are 37 unevenly spaced vertical levels in the model. Nineteen levels are in the top 1000 m, with the thickness of each model layer varying from 11 m at the surface to 198 m at 901 m. Below the top 1000 m, all levels have the same thickness, 250 m. At artificial boundaries of the model ocean, temperature and salinity are restored toward seasonal climatology. The portion of integration from which we extract the output is driven with the surface salinity restored toward the Levitus climatology (Levitus et al. 1994), the surface heat flux derived from the European Centre for Medium-Range Weather Forecasts (ECMWF) analysis, and the surface wind stress derived from the ECMWF analysis. The reader is refered to Chao et al. (1996), Carton and Chao (1999), and Pauluhn and Chao (1999) for more details of the model integration and simulation results. The model has reproduced some of the observed characteristics of the North Atlantic Ocean circulation and variability fairly well. The model GS does, however, show unrealistic features. In particular, the model GS is somewhat displaced to the north of the observed and has stronger quasi-stationary meanders along its path downstream of the separation point than does the observed (Halliwell and Mooers 1983; Watts et al. 1995). Also, the model GS underestimates kinetic energy considerably compared to some observational values at depth (Owens 1991; Richardson 1993). Farther downstream, the characteristic 90° northward turn of the current toward the northwest corner is not reproduced well in the model. Rather than turning northward, the current becomes split, producing some flow turning north and some flow shooting toward the northeast. This problem has been observed in other North Atlantic Ocean simulations by eddy-permitting or eddy-resolving models (e.g., Bryan and Holland 1989; Semtner and Chervin 1992; Smith et al. 1992; Beckmann et al. 1994). Despite these unrealistic features in the model solutions, we believe that the model output is useful for studying the processes involved in some of the features observed in the real ocean.

We focus our attention on a domain that covers 30°–60°N, 75°–15°W for the present work. The choice is made to cover most of the GS after separation from the western boundary and the North Atlantic Current (NAC) and to make diagnostic calculations reasonably efficient on our computational resources. The three-dimensional model output is saved every 3 days. This sampling frequency is sufficient to obtain smooth evolution of temperature and salinity fields, as well as the velocity field, from the saved output. The portion of the model output employed for the diagnoses is from March of year 25 to February of year 30. During this 5-yr period, 600 snapshots of potential temperature, salinity, and horizontal velocity are available. From the temperature and salinity output, we compute in situ density and potential density, using the full nonlinear equation of state used in the model integration.

3. Calculation of potential vorticity

Diagnostics based on Ertel's PV on isopycnal surfaces would be ideal for studying large-scale ocean dynamics (Rhines and Young 1982a,b). The model output, however, needs to be treated with caution when properties in the model are interpolated onto a level that is not defined naturally by the model's vertical coordinate. In this case, the model's vertical coordinate is the geometrical height, with 37 levels of uneven thicknesses. In the model, all properties are mixed uniformly within a grid cell. Therefore, calculation of Ertel's PV on isopycnal surfaces would require vertical interpolations of properties that are uniform within some vertical distance onto a height within a slab. The interpolated value is different from that of the slab within which the interpolated height exists. This is known to cause problems of spurious flux and flux divergence of various properties, unless the height scale of variation of the properties is much larger than the vertical thickness of slabs. On the other hand, QGPV on pressure surfaces does not require such vertical interpolations of the model fields since constant pressure surfaces are nearly constant in depth in the ocean. When we are primarily concerned with quasi-horizontal large-scale circulations, the quasigeostrophic framework is a simple, yet appropriate framework to use. It also enables us to diagnose the flow field with quasigeostrophic transient wave activity flux in the same framework (Nakamura and Chao 2000). Oceanic motions are quasigeostrophic to first order except in the immediate vicinity of the GS front. However, the front simulated by the model is not as sharp as is the observed and, thus, is closer to quasigeostrophy than the real flow. Indeed, with the horizontal grid spacing of the model, which is approximately 20 km, the finest resolved structure has a horizontal scale of roughly 60 km. With this horizontal scale and flow speeds of roughly 2 m s^{-1} at the maximum, Rossby

number of the flows simulated by the model is much less than 1 everywhere all the time. Also, we prefer the simpler quasigeostrophic dynamical framework to the isopycnal framework for diagnosing the model flow. For these reasons, we have chosen quasigeostrophic PV (QGPV), q, as the central quantity of the diagnoses.

Ertel's PV, P, with the hydrostatic approximation for oceanic motions may be given by

$$P = -\frac{1}{\rho}\frac{\partial \sigma}{\partial z}(f + \zeta), \tag{1}$$

where ρ is density, σ potential density, f the planetary vorticity, and ζ relative vorticity. For quasigeostrophic oceanic motions, P may be substituted by QGPV, q, defined by

$$q = \frac{\rho_0(P_0 + P^*)}{d\sigma_0/dz} \approx f + \zeta + f\frac{\partial \sigma^*/\partial z}{d\sigma_0/dz}, \tag{2}$$

where σ_0 is the reference potential density at a constant depth and $\sigma^* = \sigma - \sigma_0$ (Gill 1982). The reference PV, P_0, and deviation PV, P^*, are defined by

$$P_0 = -\frac{f}{\rho_0}\frac{d\sigma_0}{dz} \quad \text{and} \tag{3}$$

$$P^* = -\frac{f}{\rho_0}\frac{\partial \sigma^*}{\partial z} - \frac{1}{\rho_0}\frac{d\sigma_0}{dz}\left(\zeta - f\frac{\rho^*}{\rho_0}\right), \tag{4}$$

where ρ_0 and ρ^* are, respectively, the reference density and a deviation from the reference (Gill 1982). The last term on the right-hand side of Eq. (2) is the approximated form of the stretching term and may also be written as

$$-\frac{fg}{\sigma_0 N^2}\frac{\partial \sigma^*}{\partial z},$$

where N^2 is the Brunt–Väisälä frequency. Thus, q may also be written as

$$q \approx f + \zeta - \frac{fg}{\sigma_0 N^2}\frac{\partial \sigma^*}{\partial z}. \tag{5}$$

This is essentially the same as a form of QGPV familiar in much of the atmospheric literature, except for the neglected compressibility of the fluid. In practice, we compute QGPV by

$$q \approx f + \zeta + f\frac{\partial \sigma^*/\partial z}{d\sigma_0/dz}$$

from the model output at each model grid point. Relative vorticity is calculated by centered finite differencing of the velocity field at density points of the model. The reference potential density, σ_0, is calculated as the average over the entire horizontal domain and entire time series, 5 years. The time mean is computed by simply averaging the instantaneous values at each grid point over the entire 5 years first and then applying a nine-point equal-weight averaging to smooth the mean field. The reference stratification, $d\sigma_0/dz$, is calculated by centered finite differencing in the vertical at the center of each level. Perturbation stratification, $\partial\sigma^*/\partial z$, is also calculated by centered finite differencing in the vertical at the center of each level.

In comparing the mean q fields with those of mean PV, such as those reported by Keffer (1985), one has to keep in mind that there are differences between PV and q. In particular, absolute values of q are entirely different from those of PV, not to mention the units. The stretching term in q is approximated by the ratio of the perturbation stratification, $\partial\sigma^*/\partial z$, to the reference stratification at the same level, $d\sigma_0/dz$, so that it represents a normalized stretching effect at a specific level. Since q variations other than f are dominated by the stretching term, one may not see a greater absolute value of q where $\partial\sigma/\partial z$ is greater, depending on how it compares with $\partial\sigma/\partial z$ at other areas at the same vertical level. Charney and Stern (1962) showed that the dynamics of Ertel's PV on isopycnal surfaces are approximated well by dynamics of q on constant pressure surface, when the flow is quasigeostrophic. Therefore, one should focus on horizontal structures of q and quasi-horizontal structures of PV on isopycnal surfaces in comparing q and PV.

For the purpose of a direct comparison between the climatological PV fields calculated from the observed data and those generated in the model, we also calculated the time-mean Ertel's PV in a way similar to those used by Keffer (1985) and Lozier (1997). For this calculation, temperature and salinity were averaged over the 5 yr at all grid points. Then, the 5-yr averages were used to calculate the mean potential density, $\overline{\sigma}$, at all grid points. Finally, the model's climatological Ertel's PV was approximated by

$$\overline{P} = -\frac{1}{\overline{\rho}}\frac{\partial \overline{\sigma}}{\partial z}f,$$

using the centered finite differencing method for the vertical dirivative. From the 3D field of $\overline{P}$, a linear interpolation was used to approximate $\overline{P}$ on some selected isopycnal surfaces. Since the calculation procedure for $\overline{P}$ is much less demanding on computational resources, we calculated $\overline{P}$ for a large domain, 0°–65°N, 85°–10°W. We emphasize that $\overline{P}$ is used strictly for comparing the model with the observed in studying some key features in this work. A complete study of P and its fluxes on isopycnal surfaces is more desirable, but requires model output that has a higher vertical resolution or output of an isopycnal model because of the aforementioned problem of introducing spurious fluxes in the process of vertical interpolation. Such attempts will be made in the future.

4. Results and discussions

a. Characteristics of q

We examined instantaneous values of q and visualized the evolution of the q field to study its characteristics.

In general, the contribution of relative vorticity is small, 20% or less of the total value depending on the level and season. Relative vorticity is as large as 0.2×10^{-4} s^{-1} at the GS front in the top 250 m and, thus, is as large as 20% of the planetary component. However, large values of relative vorticity occur where the stretching term [the last term of Eq. (2)] is as large as or larger than the planetary component, making relative vorticity contribution practically negligible most of the time. The only exception occurs during cold months near the surface at the front of the GS.

From the surface to the bottom, there are, broadly speaking, four different patterns of q field evolution. The first is an evolution strongly characterized by the seasonal cycle near the surface down to approximately 150 m. In this shallow layer, the seasonal heating and cooling dominate the time-dependent characteristics of the q field. Very large and small values occur during warm and cold months, respectively, in the coastal region to the north of the GS. The top level where q is calculated, 17 m, shows this characteristic most clearly and is shown in Fig. 1a. Here, 1 March and 1 September of year 25 are shown to highlight the most significant characteristics in q evolution at this level, that is, the seasonal signature. Although dwarfed by the seasonal signature, there are vigorous wave motions visible in the q field also. The large values shown here arise from the greater stratification due to warming near the surface during warm months. The large q in the region is a reflection of large $\partial\sigma/\partial z$ in the region with respect to the rest of the domain. Fairly large values occur in the subtropical gyre during warm months as well. The seasonal signal of the warm period is so strong that it dominates the time-mean q field, as shown in the next section.

The second pattern is observed at levels between 150 and 1000 m. At these levels, the q field evolution is dominated by strong positive q input by the GS and mixing along the path of the GS. There still is some visible seasonal effect down to about 250 m, but it is no longer the dominant feature at these levels. An example of this pattern is shown in Fig. 1b. Since the wavelike motions are the major q evolution characteristics below the top 200 m or so, Fig. 1b through Fig. 1d show the q field on 1 March and 1 April of year 25 so that one could see the degree of deformation of water masses over one month. As an example of the second pattern, q field at 370 m is shown here since the high-q input by the model GS and meanders in the q field are most clearly visible at this level. At this level, high-q fluid injected by the GS follows the meandering path of the GS and form blobs of high q, some of which eventually form detached eddies. Intense deformation of the wavy structures results in formation of filaments and/or detached eddies, mixing high-q fluid supplied by the GS and low-q ambient fluid. As discussed later, the mean q field in this region satisfies the condition for baroclinic and barotroic instabilities, suggesting that these motions may be induced by baroclinic and barotropic instabilities. An interesting characteristic of q field evolution at these levels is eastward propagation of waves along the main path of the GS and westward propagation of waves to the south of the GS (Nakamura and Chao 2000). Detached eddies of high q to the south of the GS often propagate westward until they merge with the high-q fluid injected at the separation point. The eastward propagation of waves along the main path of the model GS is in qualitative agreement with that observed in data (e.g., Halliwell and Mooers 1983; Tracey and Watts 1986). There is no visible structure observed in the eastern half of the North Atlantic at these levels.

Farther below, from 1000 to 2500 m or so, q field shows a marked contrast to those at upper levels. At these levels, large values are seen to the east of the Mid-Atlantic Ridge (MAR), supplied by strong stratification due to the Mediterranean outflow. (The location of the MAR can be seen in Fig. 1d.) This feature is most clear at the 1375-m level and is shown in Fig. 1c. As in Fig. 1b, the q field of 1 March and 1 April of year 25 are shown to illustrate wavelike motions visible in q evolution. (Note that the model-generated Mediterranean outflow is displaced to the north of the observed.) To the west of the MAR, q values are essentially those of the planetary vorticity and the significant contribution by the GS observed at upper levels vanishes. Fluid with large q values to the east of the MAR shows much weaker motion and less mixing than the large-q fluid at upper levels in the vicinity of the GS. Although the values of q are small, fluid to the west of the MAR and near the edge of the Mediterranean outflow at these intermediate levels shows strong motion of eddies. The center of most vigorous motion at these levels is located in a region spanning 40°–50°N and 50°–30°W to the west of the MAR. This is seen, although not very clearly, in the degree of deformation of the q field there (Fig. 1c). It will be shown more clearly in particle trajectory analyses later. In fact, the eddy-driven mixing at these levels appears to be responsible for creation of a horizontally large region to the west of the MAR, extending in the vertical by approximately 1500 m, that has nearly homogenized Ertel's PV and weak gradients in q. This feature is discussed in the following section.

Finally, near the bottom, below 2500 m, the effect of the Mediterranean outflow disappears and the structure of q to the east of the MAR is dominated by the planetary vorticity. On the other hand, to the west of the MAR, the stretching term becomes important again and q field shows wavelike motions. A clear example of this is observed at the 2875-m level and is shown in Fig. 1d. At these levels, the center of the action is again located between 40° and 50°N to the west of the MAR, below a northern branch of the model GS. Again, this is seen to some extent in Fig. 1d in the degree of q-field deformation, but will be shown more clearly in particle trajectory analyses later.

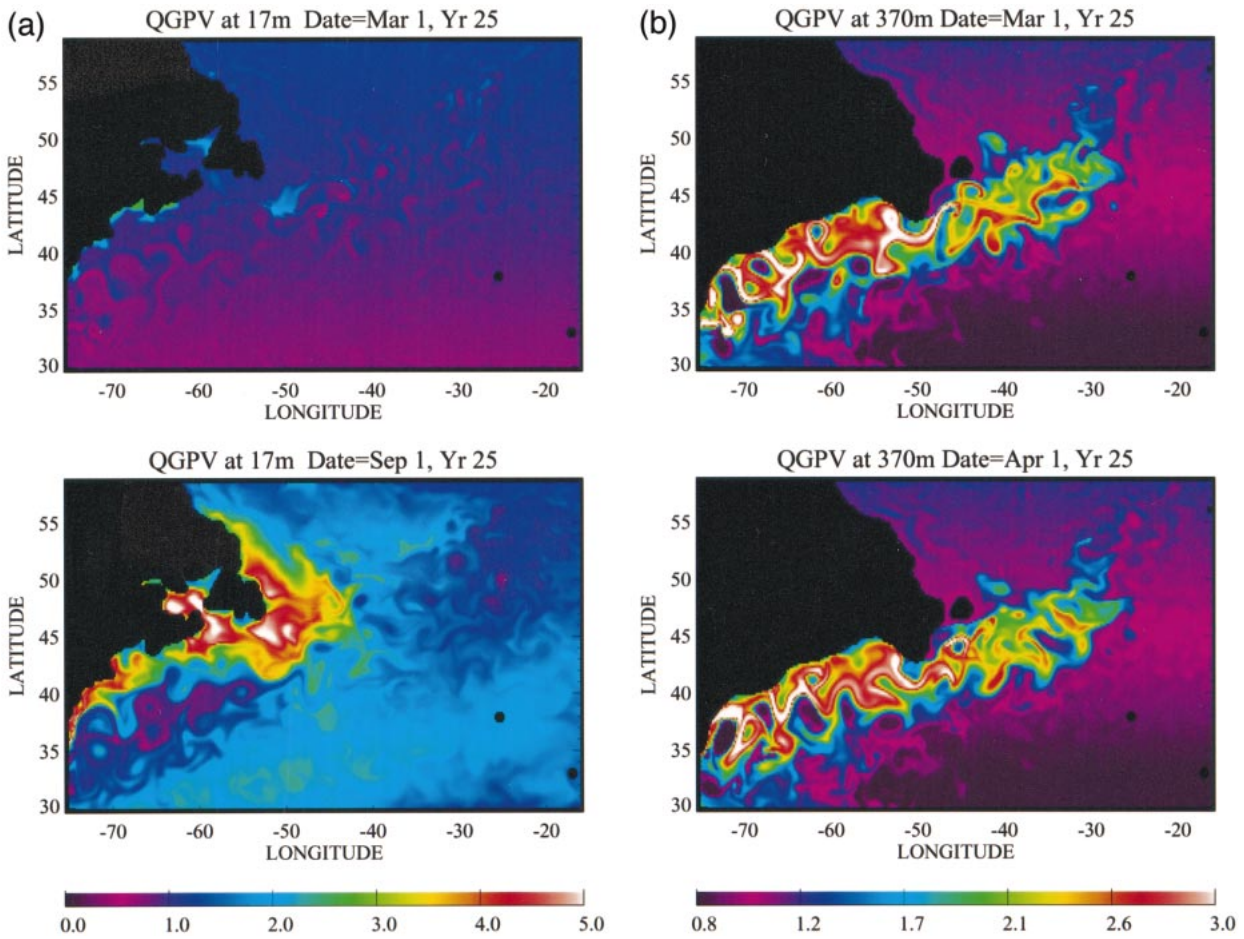

FIG. 1. Snapshots of q at (a) 17 m, (b) 370 m, (c) 1375 m, and (d) 2875 m in the model. (a) Here 1 Mar and 1 Sep of year 25 illustrate the large seasonal changes. (b), (c), and (d) Here 1 Mar and 1 Apr of year 25 highlight wave-induced deformation of q field over a

b. Mean q fields

1) MIXED LAYER

The time-mean q and horizontal flow at 17 m are shown in Fig. 2. The structure shown here is representative of the top 100 m or so. In these shallow layers that are vertically well mixed most of the year, the $\overline{q}$ structure is dominated by the seasonal effect. A particularly conspicuous seasonal effect is observed in the shallow region near the coast. Very large values in q are attained in this region during warm months through the stretching term and are still reflected in the time mean. There is a large input of q by the GS from the vicinity of the separation point, but dwarfed by the seasonal effect in this figure. The contribution of relative vorticity is negligible, even at the front of the GS, compared to the stretching term. Instantaneous values of relative vorticity can be as large as 0.2×10^{-4} s^{-1} at these levels where the flow speed is large, but the time-mean values are an order of magnitude smaller since the relative vorticity term tends to cancel out when averaged over time.

2) THE THERMOCLINE AND A TONGUE OF LARGE $\overline{q}$

At around 140 m, the structure of $\overline{q}$ begins to show a transition to another characteristic pattern (Fig. 3). At this level, the strong q input by the GS begins to appear as a major contributor, while the seasonal effect near the coast in shallow areas is still significant. The region of large $\overline{q}$ also begins to show a tonguelike structure, elongated in the east-northeast direction from the separation point along the model GS. At this level, the tongue is not as clear as that at deeper levels and appears as a band of high $\overline{q}$ along the model GS with its tip protruding as a small tongue off of Newfoundland. To the south of the band of large $\overline{q}$, there is a large ''island'' of small $\overline{q}$ with a similar orientation. Although the region of small $\overline{q}$ resembles the ''island'' of small PV at a corresponding σ level shown by Keffer (1985, his Fig. 4), the model mean potential temperature does not suggest that the island of small $\overline{q}$ is associated with the 18° Water of Worthington (1959) to which Keffer (1985) attributes the island of small PV. The structure of $\overline{q}$ at 370 m clearly shows the effect of the GS on $\overline{q}$ (Fig. 4).

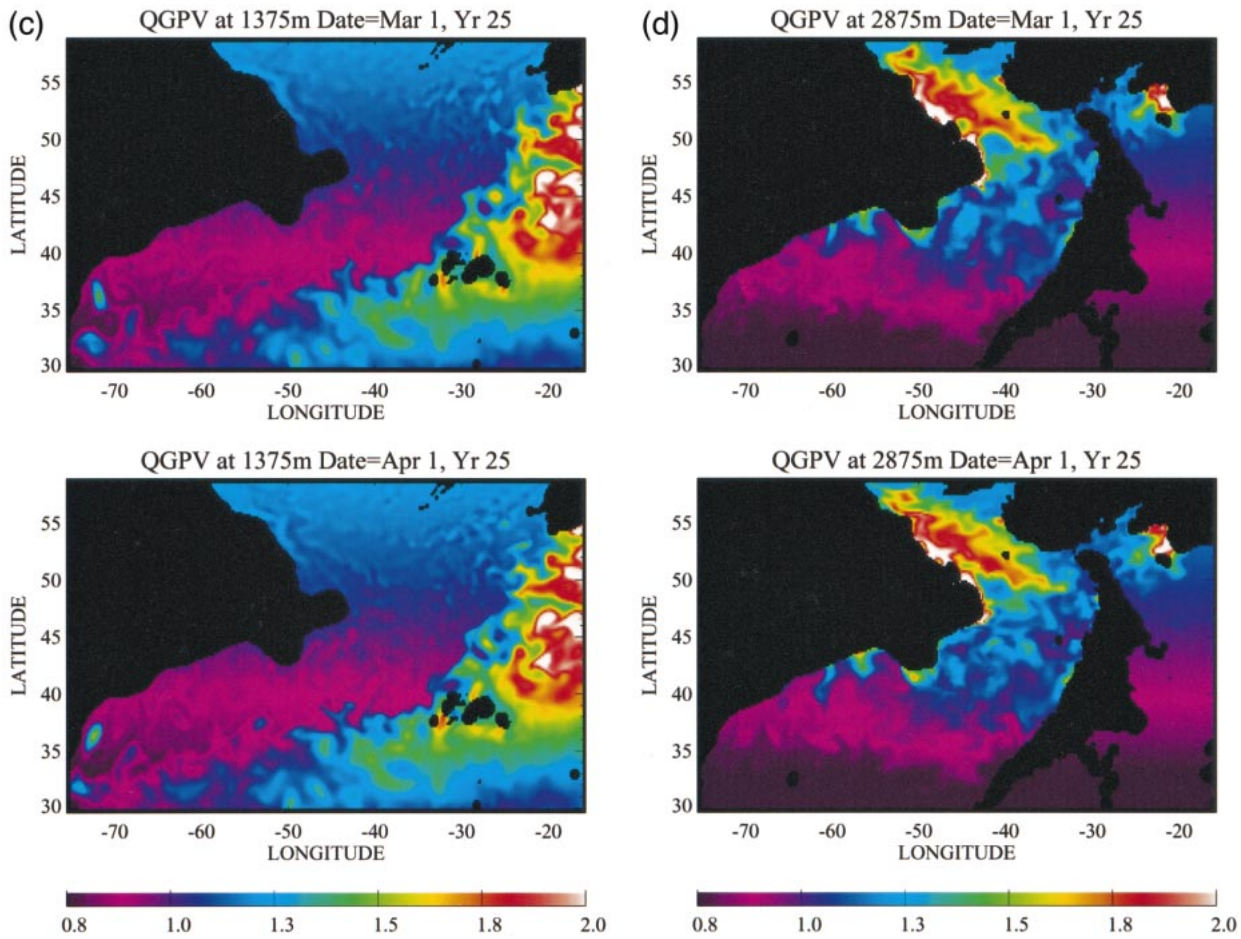

FIG. 1. (*Continued*) period of one month. Units of q are 1×10^{-4} s^{-1}.

A strong q input by the GS is responsible for the zonally elongated region of large $\overline{q}$ with the maximum just south of the coast. The effect of the GS is visible as far downstream as 55°N, 30°W. Note that to the north of the center of the tongue of large $\overline{q}$, the sign of the meridional gradient of $\overline{q}$ is negative. This characteristic structure of $\overline{q}$ becomes even more prominent at slightly deeper levels, as shown in Fig 5.

At 577 m, the $\overline{q}$ field clearly shows the presence of an island of large $\overline{q}$, indicated by the closed contours of $\overline{q}$ within a tongue of high $\overline{q}$ (Fig. 5). This tongue of large $\overline{q}$ is clearly visible at 721 and 901 m, but shifts southward with depth and eventually disappears at around 1000 m. Maps of PV for intervals σ_θ = 26.5–27.0, σ_θ = 27.0–27.3, and σ_θ = 27.3–27.5 by Keffer (1985) all show a tongue of large PV elongated along the path of the GS. These intervals in the Levitus data lie between 100 and 1000 m in the region considered for the model diagnoses. The tongue in Keffer's figures also show some sign of southward shift with depth. These structures are present in $\overline{P}$ calculated from the 5-yr mean potential temperature and salinity in the model. Figure 6 shows $\overline{P}$ on a surface of $\overline{\sigma}_{\text{surface}}$ = 27.15 calculated from the model output in a manner described in section 3. There is a broad agreement in the structure between $\overline{P}$ shown in Fig. 6 and that calculated by Keffer for the interval $\overline{\sigma}_{\text{surface}}$ = 27.0–27.3 in the western North Atlantic. Mechanisms through which the tongue of large $\overline{P}$ and the tongue of large $\overline{q}$ are generated are probably the same. Plots of q fluxes by the mean flow and eddies show that the mean jet of the GS is primarily responsible for advecting large q from the western boundary along the model GS (Fig. 7). Figure 7 shows the center of the tongue of high $\overline{q}$ coinciding with either the primary or the secondary branch of the model GS. The values of $\overline{q}$ decrease toward downstream along the mean GS, suggesting that eddy mixing and/or diabatic processes are diffusing q as the high-q waters are advected downstream by the mean flow. Essentially all of the large q fluxes arise from advection of highly stratified (with respect to the other parts of the domain) water by the model GS. While the eddy fluxes of q are much smaller than the mean fluxes, convergences of the mean and eddy fluxes are comparable in magnitude and tend to cancel out each other (not shown). The advection of high-q waters by the GS here is responsible for main-

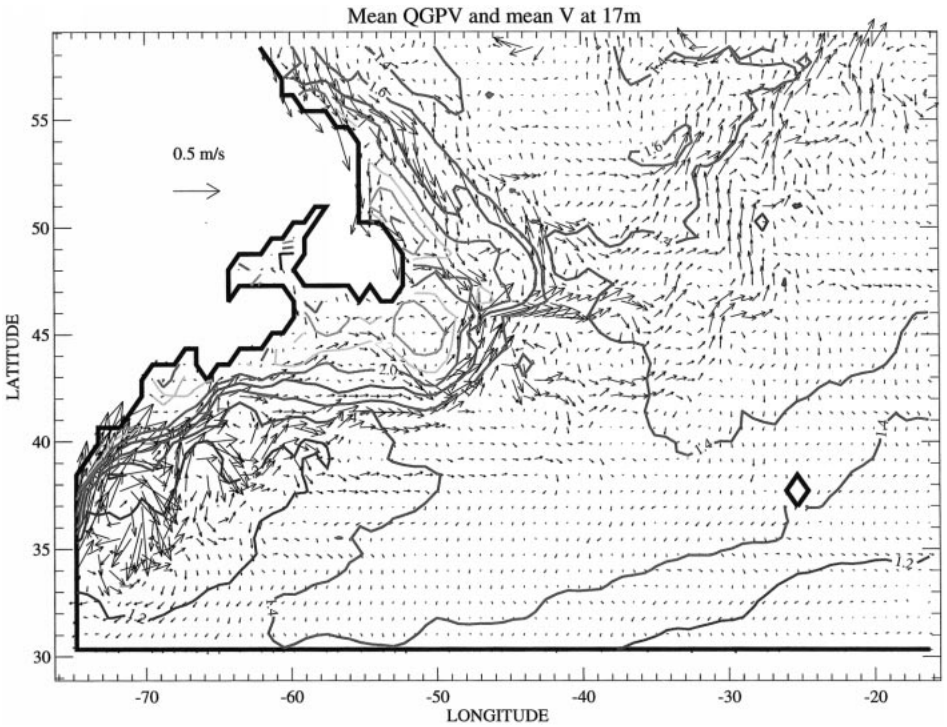

FIG. 2. Contours of $\overline{q}$ and vectors of $\overline{\mathbf{V}}_h$ at 17 m. Units of $\overline{q}$ and $\overline{\mathbf{V}}_h$ are, respectively, 1×10^{-4} s^{-1} and m s^{-1}. The contour interval for $\overline{q}$ is 0.2. Thick contours mark the topographic boundary.

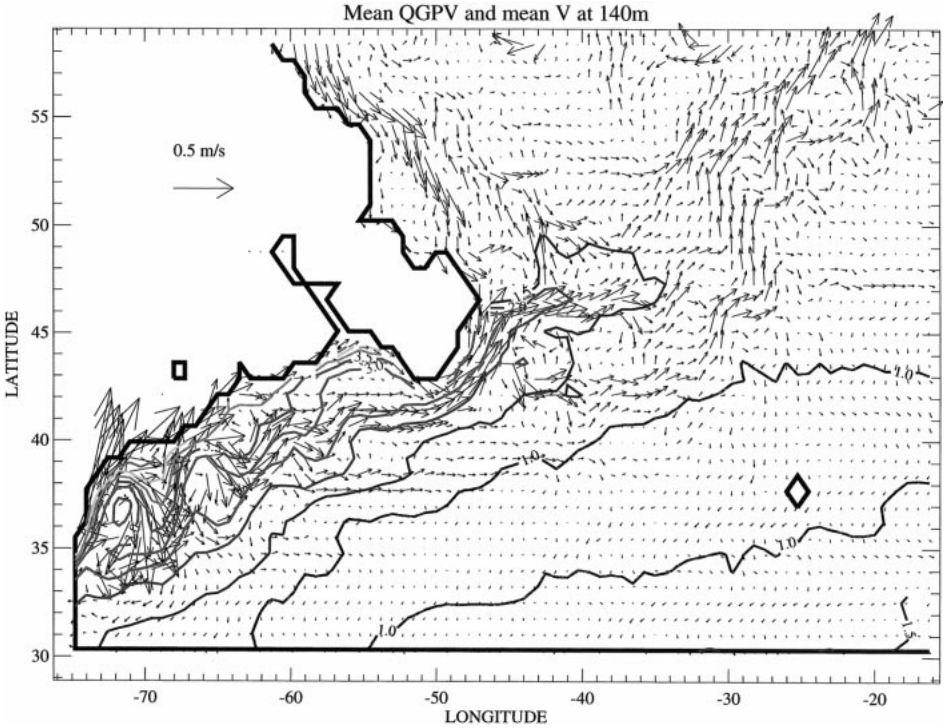

FIG. 3. Same as in Fig. 2 but for 140-m level. The contour interval for $\overline{q}$ is 0.5.

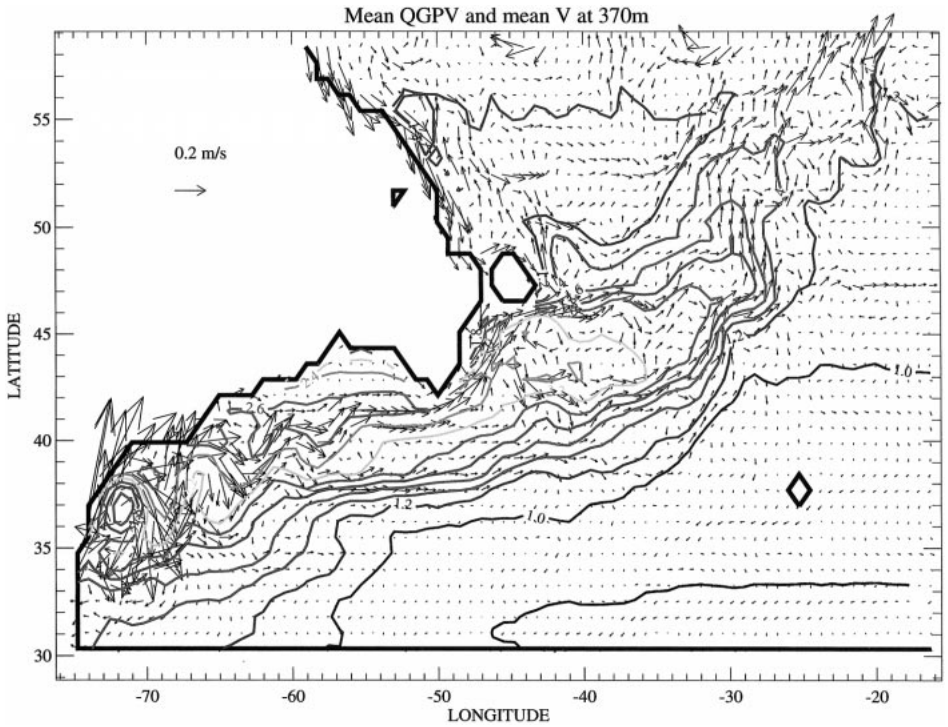

FIG. 4. Same as in Fig. 2, but for 370-m level. The contour interval for $\overline{q}$ is 0.2.

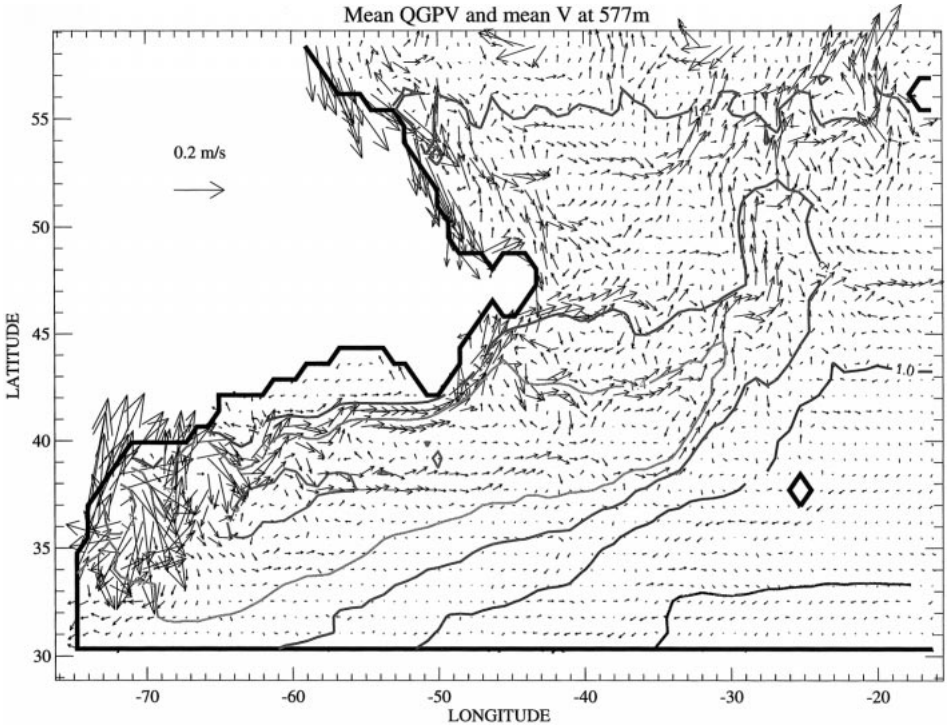

FIG. 5. Same as in Fig. 2 but for 577-m level. The contour interval for $\overline{q}$ is 0.2.

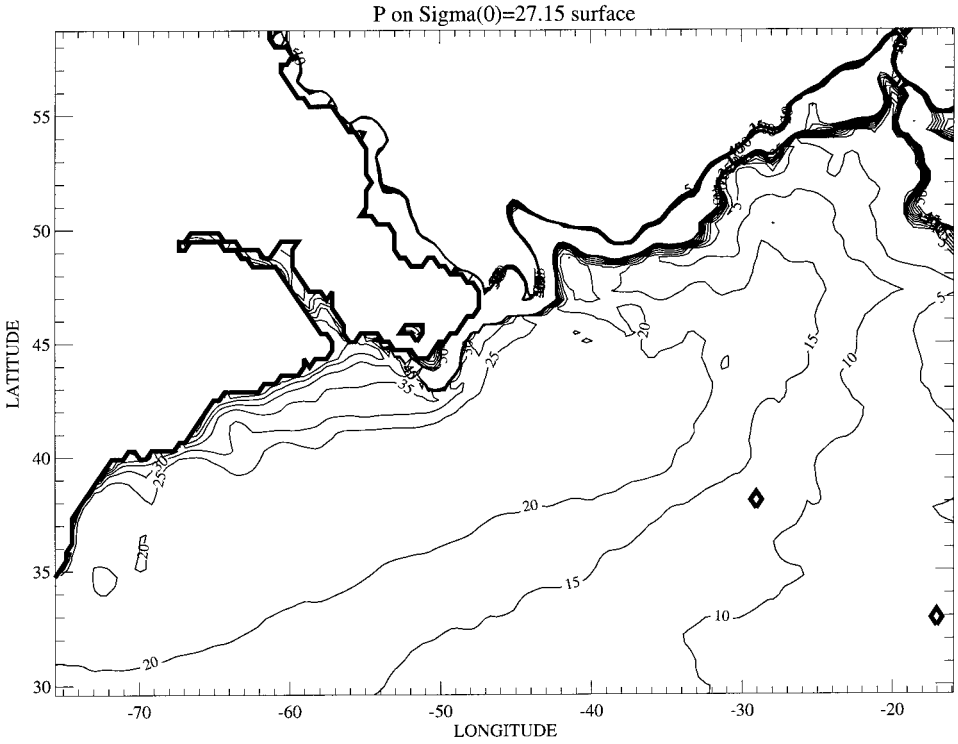

FIG. 6. Contours of $\overline{P}$ on the surface of $\overline{\sigma}_{\text{surface}} = 27.15$. The units of $\overline{P}$ are 1×10^{-11} m^{-1} s^{-1}. The contour interval is 5. Thick contours mark the topographic boundary.

taining the condition that supports baroclinic and barotropic instabilities, as manifested by the vertical and horizontal structures of QGPV gradient in the vicinity of the tongue of high $\overline{q}$. An intriguing aspect of the tongue of high $\overline{q}$ and $\overline{P}$ is that there is no sign of high $\overline{P}$ originating from farther south upstream of the GS.[1] The tongue appears to originate from the western boundary. We speculate that the source of high $\overline{q}$ and $\overline{P}$ is actually a combination of local upwelling of relatively dense water along the western boundary near the separation point and advection of light water by the GS, which would intensify stratification and, hence, tend to increase q and P.

To examine the role of the mean flow and eddy advection in the elongated tongue of large $\overline{q}$, we calculated trajectories of particles, using the model flows at 577 m. The trajectories were calculated by a scheme that uses the standard fourth-order Runge–Kutta method with a linear interpolation of available flow field in time and space. Horizontal flows at 577 m are used for these calculations, rather than flows interpolated onto an isopycnal surface, to be consistent with the quasigeostrophic framework used in the current study. At this level, it is likely to introduce some spurious paths, despite a fairly large model layer thickness, which is 128 m at this level. Particularly, when a particle is displaced a great distance in the meridional direction, it may cross over to an isopycnal surface that lies in another model level. Also, a horizontal displacement across the model GS, although the model front is not as sharp as that of the real GS, is likely to be associated with a substantial vertical displacement along isopycnal surfaces. Although the current diagnoses focus on q at constant depths and, thus, the use of horizontal flow for trajectory calculations is consistent with the framework, some caution is advised to account for this uncertainty. We calculated trajectories of 100 particles released from ten different $2° \times 2°$ areas in the domain. The particles are uniformly spread within the area of release at the beginning. The sites of particle release were chosen to cover the tongue of large $\overline{q}$ and a variety of characteristics in the mean flow. For each initial particle release site, we ran a pair of 5-yr trajectory calculations; one with the full flow and the other with the mean flow. The ten areas of particle release and the mean trajectory length for each run are given in Table 1. Five pairs of the 10 runs are shown as representative examples in Figs. 8–12. The areas of particle release for the runs shown in Figs. 8–12 are, in the same order, area 1, area 2, area 3, area 6, and area 9. Area 1 is located in the core of the model GS before it splits into two branches.

[1] As mentioned in section 3, $\overline{P}$ was calculated for a larger domain, 0°–65°N, 85°–0°W. Here, however, $\overline{P}$ is shown for the same domain as that for $\overline{q}$ for an easier comparison.

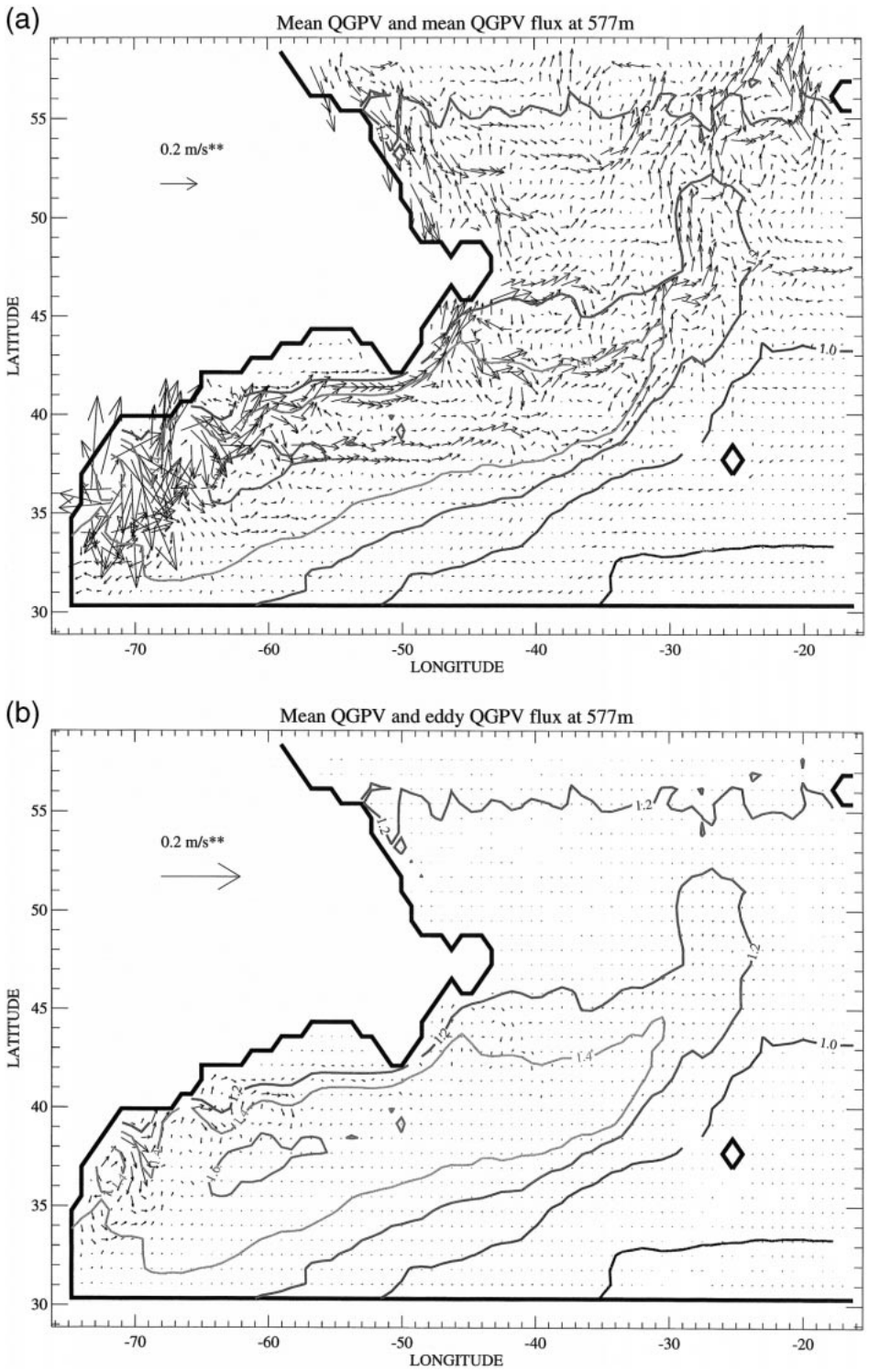

FIG. 7. Contours of $\overline{q}$ and vectors of (a) $\overline{\mathbf{V}}_h\overline{q}$ and (b) $\overline{\mathbf{v}_h'q'}$ at 577 m. The units and contour interval for $\overline{q}$ are the same as in Fig. 5. The units of $\overline{\mathbf{V}}_h\overline{q}$ and $\overline{\mathbf{v}_h'q'}$ are m s^{-2}. Thick contours mark the topographic boundary.

TABLE 1. Trajectory calculation initial particle release area number, release site location, flow used for particle advection, and the mean trajectory length of 100 particles. The release location is indicated by longitudinal and meridional extent in degrees. The mean trajectory length is given in kilometers. The flow used for these cases is from the model 577-m level. See text for details.

Area	Initial position		Flow type	Mean pathlength
	Lat (°N)	Long (°W)		
1	35–37	68–70	Full	16 966
1	35–37	68–70	Mean	7929
2	35–37	58–60	Full	14 097
2	35–37	58–60	Mean	2390
3	35–37	48–50	Full	7512
3	35–37	48–50	Mean	1414
4	35–37	38–40	Full	6806
4	35–37	38–40	Mean	980
5	39–41	63–65	Full	16 623
5	39–41	63–65	Mean	6518
6	39–41	53–55	Full	14 919
6	39–41	53–55	Mean	4148
7	39–41	43–45	Full	12471
7	39–41	43–45	Mean	4323
8	39–41	33–35	Full	10778
8	39–41	33–35	Mean	2814
9	43–45	43–45	Full	15438
9	43–45	43–45	Mean	7623
10	43–45	33–35	Full	14414
10	43–45	33–35	Mean	7591

Area 2 is located in the center of an island of large $\overline{q}$, marked by a closed contour of $\overline{q} = 1.6 \times 10^{-4}$ s^{-1}, where the mean flow is relatively weak. Area 3 is located to the south of the center of the tongue of large $\overline{q}$, just to the south of the secondary branch of the model GS. Area 6 is located immediately to the north of the center of the tongue of large $\overline{q}$ and sits in the primary branch of the model GS. Finally, area 9 is located near the northen edge of the tongue of large $\overline{q}$ enclosed by the contour of $\overline{q} = 1.2 \times 10^{-4}$ s^{-1} in the primary branch of the model GS.

From the ten pairs of trajectory calculations, we have found that the trajectories generally tend to ''paint out'' the area of the tongue of large $\overline{q}$ downstream of the site of particle release, when the particles are advected with the full flows and the particles are released within the tongue (Figs. 8, 9, 11, 12). An exception is the case shown in Fig. 10. In this case, particles tend to remain in the southern half of the tongue. Trajectories calculated with the mean flow, on the other hand, show much smaller particle spread in general. The large difference in the particle spread between the cases with the full flow advection and the mean flow advection indicates the importance of eddy mixing in formation and maintenance of the broad tongue of large $\overline{q}$ at these levels.[2]

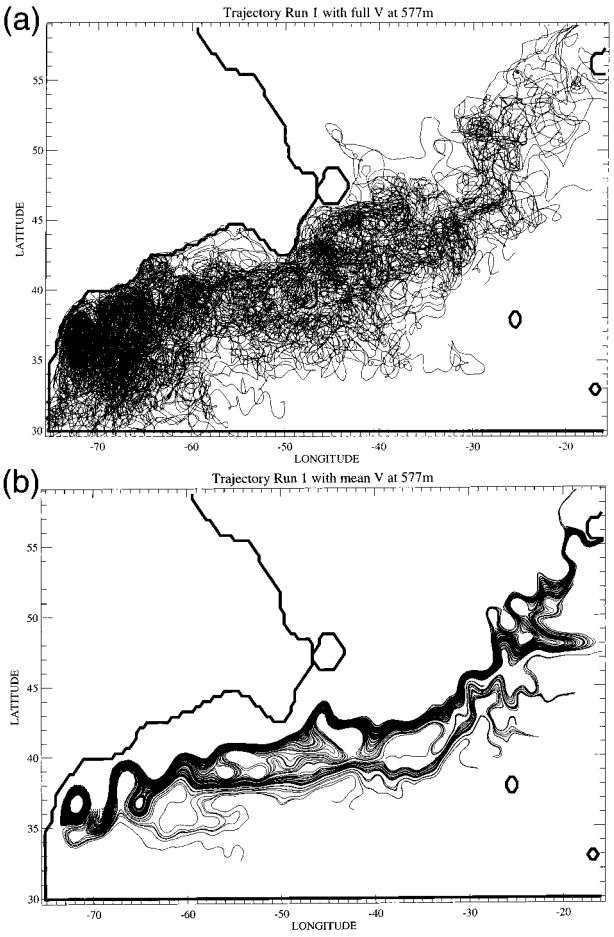

FIG. 8. Trajectories of 100 particles released from a 2° × 2° area covering 35°–37°N, 70°–68°W (area 1). The particles are evenly spaced at the beginning and then advected by (a) the full flow or (b) the mean flow at 577 m for 5 yr. Thick contours mark the topographic boundary.

The trajectories calculated by the mean flow also show much smaller downstream movement of particles compared to those calculated with the full flows. Exceptions occur when the particles are released from the core of the primary branch of the model GS (Figs. 8, 11, 12). In these cases, the particles are advected quickly by the mean GS over a long distance along the tongue of large $\overline{q}$. To crudely assess the contribution of the mean flow and eddies in advection of the particles, we calculated the average pathlength traveled by a particle during the trajectory calculations. For the cases shown in Figs. 8–12, in the same order, the average path lengths are the following: 16 966 km with the full flow and 7929 km with the mean flow, 14 097 km with the full flow and 2390 km with the mean flow, 7512 km with the full flow and 1414 km with the mean flow, 14 919 km with the full flow and 4148 km with the mean flow, 15 438 km with the full flow and 7623 km with the mean flow. The averages for all ten trajectory runs are 13 002 km with the full flow and 4573 km with the

[2] One must note that the separation of the total flow into the time mean and eddy does not have any physical basis and is not synonymous to the separation into a steady basic flow and waves. The time-mean flow shown here is highly likely to contain wave flows; thus, the difference in the mixing shown in these figures is likely to underestimate the effect of waves in mixing.

mean flow. The ratio of the two is approximately 2.8 to 1. The ratio suggests that the contribution of eddies in particle advection is about twice larger than the mean flow in these calculations. The rapid mixing shown here is in agreement with the results reported by Cox (1985), Böning and Cox (1988), and Rhines and Schopp (1991). Böning and Cox (1988) also noted that the mean flow is important in large-scale transport, while eddy mixing is effective in shaping the mean PV structure. The calculations shown here appear to support their results also. In most of the cases that show large particle spread or strong advection, many particles are found to move out of the tongue, crossing contours of $\overline{q}$ into smaller $\overline{q}$ values. It suggests that there must be some dissipation of q through mixing with small-q waters and/or diabatic processes occuring while the particles are advected. These trajectories and q flux patterns suggest that the tongue is a product of strong q input and advection by the GS, mixing by eddies along the path of the GS, and dissipation of q.

3) Intermediate layers and a pool of nearly homogenized PV

Below 1000 m in the model, $\overline{q}$ field shows another major change (Fig. 13). The tongue of large $\overline{q}$ along the GS disappears below 1000 m and the effect of the Mediterranean overflow on stratification emerges to the east of the MAR where large values of $\overline{q}$ with strong gradients are seen. (The model Mediterranean overflow is displaced to the north of the observed.) The center of the MAR is aligned north–south, with a slight northeast tilt, at around 30°W. In contrast, the $\overline{q}$ field to the west of the MAR shows small values, mostly consisting of f and weak gradients. These characteristics are particularly pronounced from 1375 to 2375 m. The strong direct influence of the GS on $\overline{q}$ observed in the top 1000 m mostly disappears except for a small ''island'' of relatively large $\overline{q}$ at the separation point around 37°N (Fig. 13). The ''island'' disappears below the 1375-m level. Also, at 1375 m, an ''island'' of relatively small $\overline{q}$, indicated by the contour of $\overline{q} = 0.9 \times 10^{-4}$ s^{-1}, exists (Fig. 13). It appears to be created by mixing near the separation point. At these levels, contributions of the stretching term and ζ to the west of the MAR are negligible, leaving f to dominate the $\overline{q}$ field. We will refer to the $\overline{q}$ structure dominated by f as ''weakly varying $\overline{q}$.'' The smallness of the stretching term to the west of the MAR is due to the very weak stratification there and strong stratification to the east of the MAR. These horizontal structures of the $\overline{q}$ field are remarkably similar to those reported by Lozier (1997), who calculated the climatological PV for the North Atlantic using an improved hydrographic dataset (Lozier et al. 1995). Lozier showed that the large region of nearly homogenized PV in her dataset is encircled by a large recirculation and speculated that the near-homogenization of PV is due to eddy mixing. (Unless stated otherwise, we will use weakly varying and ''nearly homogenized'' to refer to the horizontal or quasi-horizontal structures of PV and QGPV in the following.) Although the model-produced mean flow is considerably noisier than that shown by Lozier (1997), there are some signs of a similar large recirculation at these levels in the model as well. It will be shown in trajectory calculations to be discussed later. The model $\overline{P}$ also shows the pool of nearly homogenized PV at these levels, particularly clearly on the surface of $\overline{\sigma}_{2125\text{m}} = 37.5$ (Fig. 14). For comparison, $\overline{q}$ at 1875 m is shown in Fig. 15.[3] The pool of nearly homogenized $\overline{P}$ shows up as a pool of weakly varying $\overline{q}$ here. The initial condition used to start the model integration used for this study does not

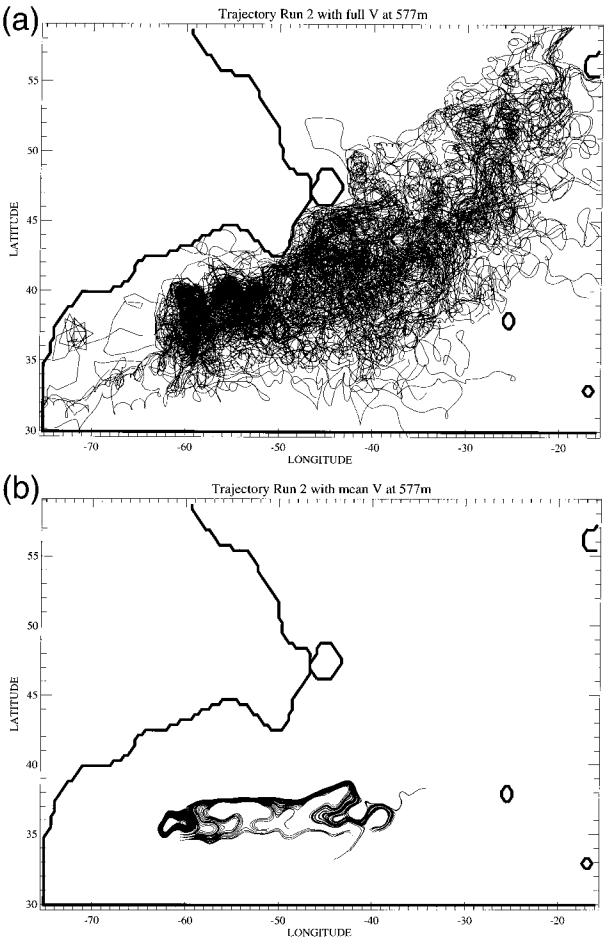

FIG. 9. Same as in Fig. 8 but for particles that are initially located in a 2° × 2° area covering 35°–37°N, 60°–58°W (area 2).

[3] The isopycnal surface of $\overline{\sigma}_{2125\text{m}} = 37.5$ lies between 1800 and 2200 m in most of the domain and outcrops in the sinking region. However, the sinking region in the model shows nearly zero stratification in the top 2500 m or so; thus, one may consider the surface to be lying at around 2000 m in the entire domain for practical purposes.

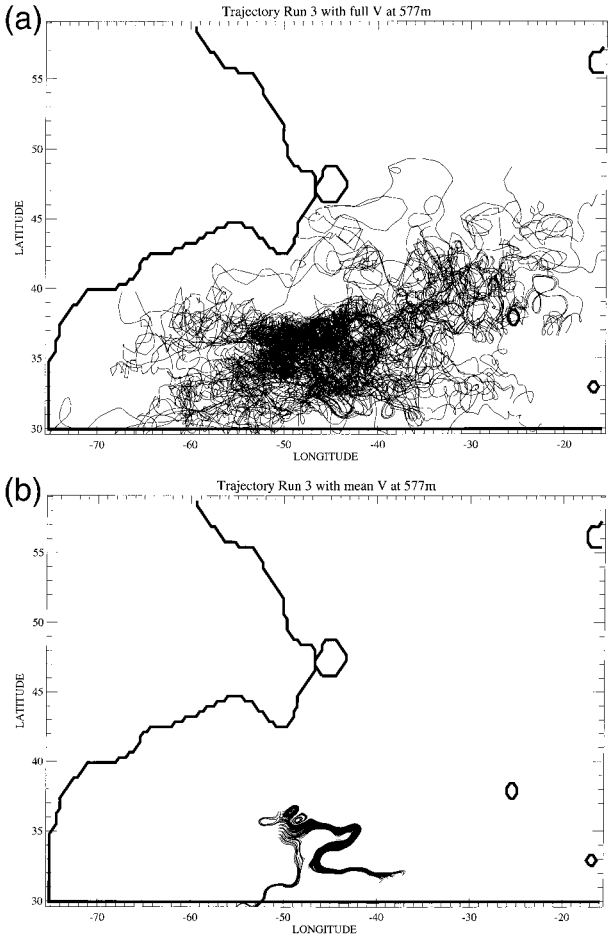

FIG. 10. Same as in Fig. 8 but for particles that are initially located in a 2° × 2° area covering 35°–37°N, 50°–48°W (area 3).

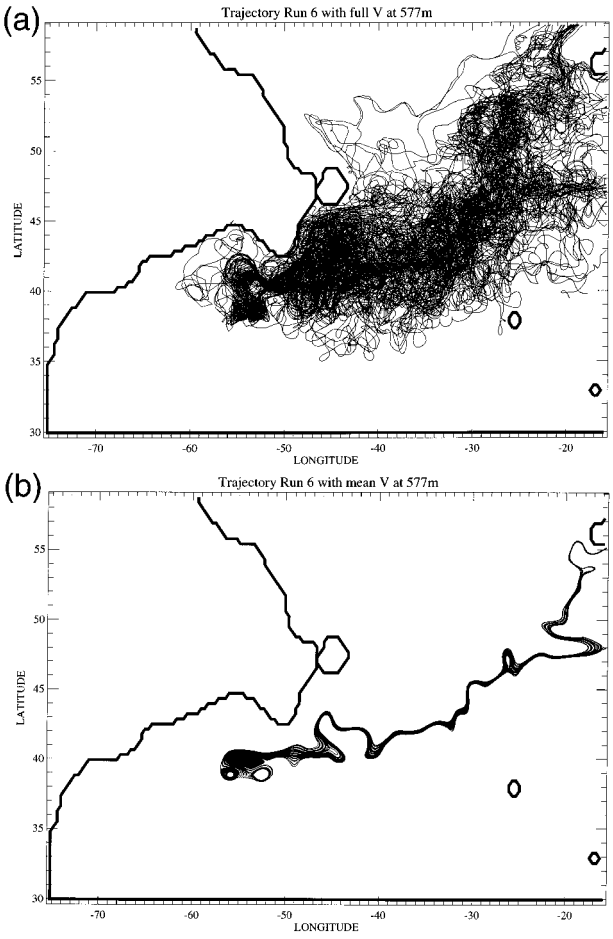

FIG. 11. Same as in Fig. 8 but for particles that are initially located in a 2° × 2° area covering 39°–41°N, 55°–53°W (area 6).

have these structures, implying that the structures are generated by the model dynamics. The region of weakly varying $\overline{q}$ has a vertical extent of 1000–1500 m and appears as a deep pool of weakly varying $\overline{q}$ in vertical cross sections. Similarly, the corresponding $\overline{P}$ field shows a deep pool of nearly homogeneous $\overline{P}$ at slightly deeper levels. Example vertical cross sections of $\overline{q}$ and $\overline{P}$ are shown in Fig. 16. This latitude, 40°N, is chosen here because the main branch of the model GS at upper levels flows eastward at this latitude. The vertical structure is very similar to a deep layer of nearly homogenized PV in the same region found by Lozier in her improved hydrogrphic data (Lozier 1999). This region of the pool is characterized by a $\overline{q}$ field that shows a favorable condition for baroclinic wave growth (Fig. 17) and indeed shows vigorous transient wave activity in the thermocline and deep layers (Nakamura and Chao 2000). The thick layer of weakly varying $\overline{q}$ lies underneath a layer of strong positive meridional gradient of $\overline{q}$, followed by a layer of weaker negative gradient below. It also lies above a layer of weak positive meridional gradient of $\overline{q}$. This structure satisfies the condition required for baroclinic instability. Examination of the meridional gradient of $\overline{P}$ on several isopycnal surfaces suggest that the condition is met in the $\overline{P}$ field as well (not shown).

Lindzen (1993) suggests that the midlatitude atmosphere's tendency toward baroclinic neutrality may create a layer of fluid with horizontally homogenized PV and that the depth of the layer is determined by the vertical scale of the largest unstable baroclinic waves in the system. He argues that the baroclinic basic state of the Eady problem (Eady 1949), characterized by concentrated QGPV gradients at the top and the bottom of a fluid with zero QGPV gradient in the interior, is baroclinically neutral when the minimum horizontal wavenumber is sufficiently large to suppress interactions between the disturbances at the top and the bottom. In his argument, the interior layer of zero QGPV gradient, in which the edge waves at the bottom and the top decay exponentially, is a crucial factor in establishing the neutrality of the basic state that has a strong PV gradient at the top and the bottom of the fluid. If baroclinic flows indeed tend toward baroclinic neutrality, wave-induced

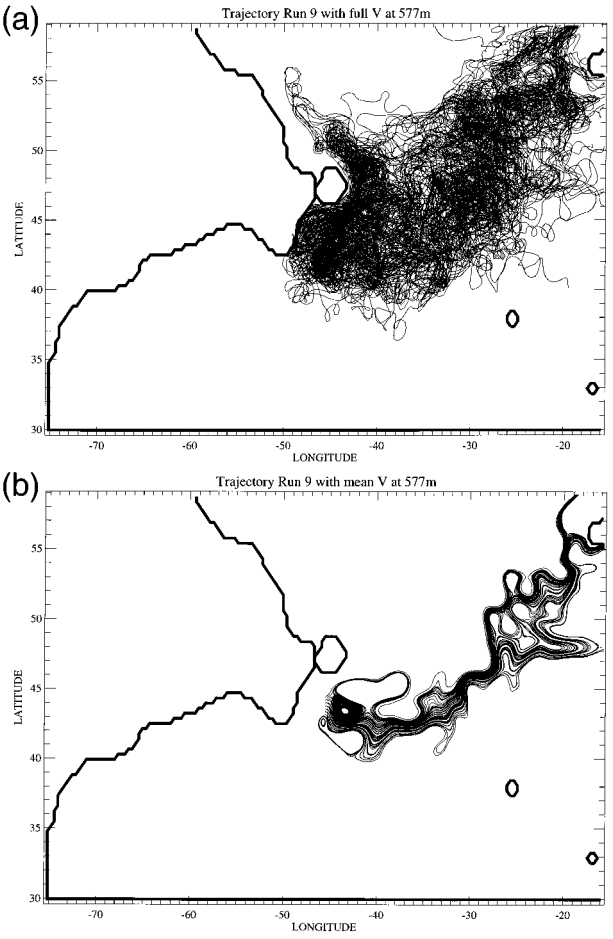

FIG. 12. Same as in Fig. 8 but for particles that are initially located in a 2° × 2° area covering 43°–45°N, 45°–43°W (area 9).

mixing generated by baroclinic instability may create such a layer of horizontally homogeneous PV in the interior of the baroclinic fluid. In the atmosphere, such an interior layer of nearly homogenized PV, troposphere, indeed exists. Comparisons of the critical meridional temperature gradient for baroclinic instability in a two-layer model and the observed meridional temperature gradient by Stone (1978) also suggest that baroclinic eddies tend to bring the background state toward baroclinic neutrality in midlatitudes. Based on his argument, Lindzen (1993) used the Eady's shortwave cutoff relationship to estimate fairly well the depth of the troposphere, in which PV is nearly homogenized. The Eady's shortwave cutoff gives

$$|\mathbf{K}|^2 \leq (2.34)^2 \frac{f^2}{N^2 H^2}, \tag{6}$$

where $\mathbf{K}$ is the total wavenumber of baroclinic waves and H is the depth of fluid with rigid boundaries at the top and the bottom (e.g., Lindzen 1993). Lindzen (1993) relates H to the depth of the troposphere, based on the similarity between the characteristic distribution of horizontal QGPV gradient in the Eady's model and the troposphere. An assumption of a rigid lid at the top of the fluid, used in the Eady's model, is more applicable to oceans than the atmosphere. Also, we consider the zonal basic flow with infinite meridional extent used in the Eady's model as an acceptable idealization of the basic state centered at the GS.

Based on the above arguement, we have estimated the depth of the layer of homogenized $\overline{P}$ or weakly varying $\overline{q}$, using the Eady shortwave cutoff relation. In the model ocean, the volume-weighted vertical average of N^2 to the west of the MAR has a typical value of 5×10^{-6} s^{-2}. At these latitudes, f is approximately 1×10^{-4} s^{-1}. Thus, from the above equation, we obtain

$$H_c^2 \approx \frac{0.0110}{|\mathbf{K}_c|^2}, \tag{7}$$

where H_c is the depth of fluid through which PV is homogenized by the longest unstable baroclinic waves with the total wavenumber $\mathbf{K}_c$. For simplicity, we use zero wavenumber in the meridional direction and set $\mathbf{K}_c = k_c = 2\pi/L_c$, where L_c is the wavelength of the longest unstable baroclinic waves supported in the vicinity of the GS. With this simplification, we obtain

$$H_c \approx 0.016 L_c. \tag{8}$$

In reality, unstable baroclinic waves are not likely to neutralize the mean flow, but are likely to achieve a nonlinear balance with the mean flow and continuous forcing that supplies baroclinic or potential energy for the eddies to feed upon. In maintaining such a balance, the most unstable baroclinic waves are likely to play the key role. Based on this assumption, we estimate H_c by using the scale of Rossby deformation radius for L_c. Since the model has a horizontal grid spacing of about 20 km in this region, the unstable baroclinic waves resolved in this region have wavelength on the order of 100 to 150 km, essentially a model-imposed deformation radius. With these numbers, we obtain crude estimates of the depth of the nearly homogenized PV to be in a range of 1600 to 2400 m, which are not very far from the depth of nearly homogenized $\overline{P}$ or weakly varying $\overline{q}$ in the model output. The vertically extended region of nearly homogenized $\overline{P}$ and weakly varying $\overline{q}$ may be explained by the theory that a baroclinic ocean tends toward a state of baroclinic neutrality. Creation of a vertically extended region of horizontally homogenized QGPV is also shown in midlevels of idealized wind-driven ocean circulation models (Holland et al. 1984; Rhines and Schopp 1991). In these idealized models of wind-driven circulation, the homogenization is accomplished by strong eddy mixing induced by interfacial form drag. A calculation of the vertical component of transient wave activity fluxes, using the model output diagnosed here, shows predominantly downward fluxes below the top 1000 m, suggesting that the same mechanism is operating in this model (Nakamura and Chao 2000). Finally, we note that the baroclinic neutrality

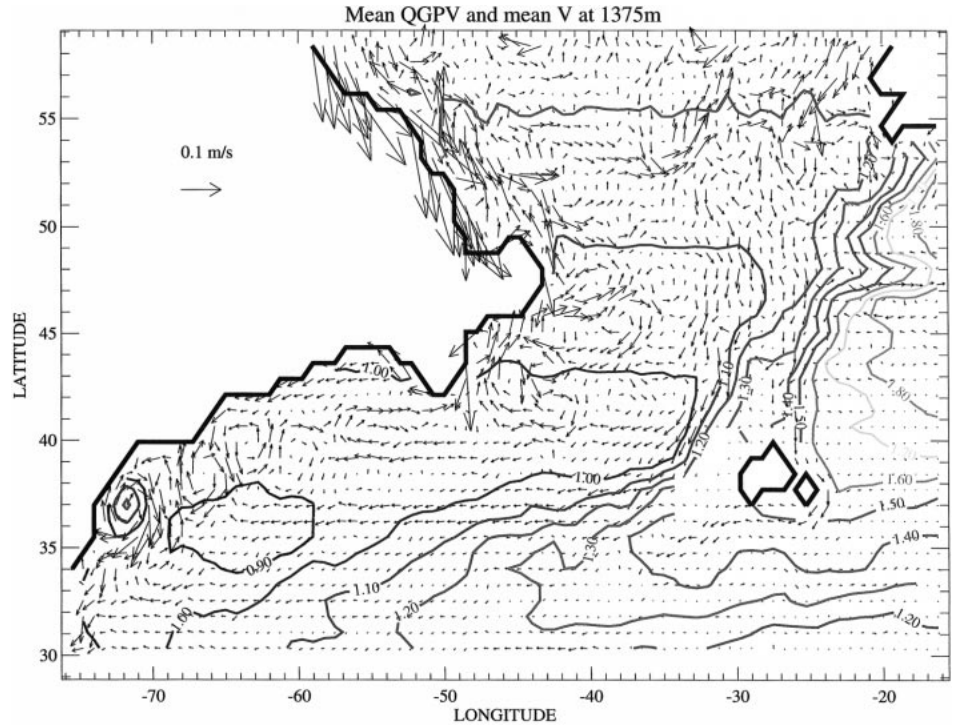

FIG. 13. Same as in Fig. 2 but for the 1375-m level. Contour interval for $\overline{q}$ is 0.1.

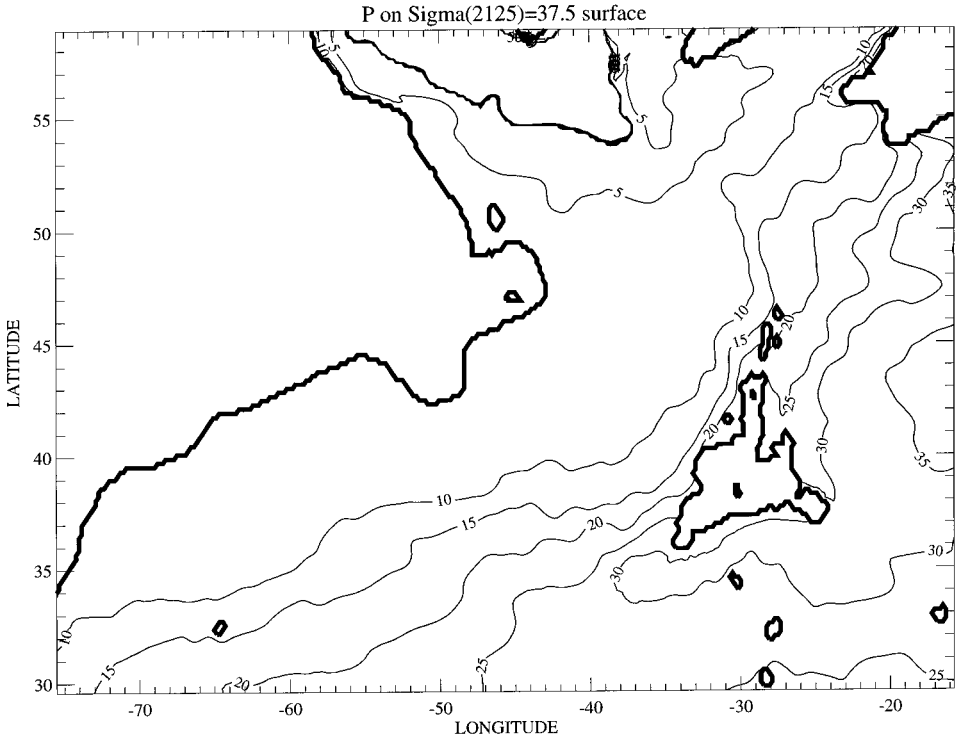

FIG. 14. Contours of $\overline{P}$ on the surface of $\overline{\sigma}_{2125\mathrm{m}} = 37.5$. The units of $\overline{P}$ are 1×10^{-12} m^{-1} s^{-1}. The contour interval is 5. Thick contours mark the topographic boundary.

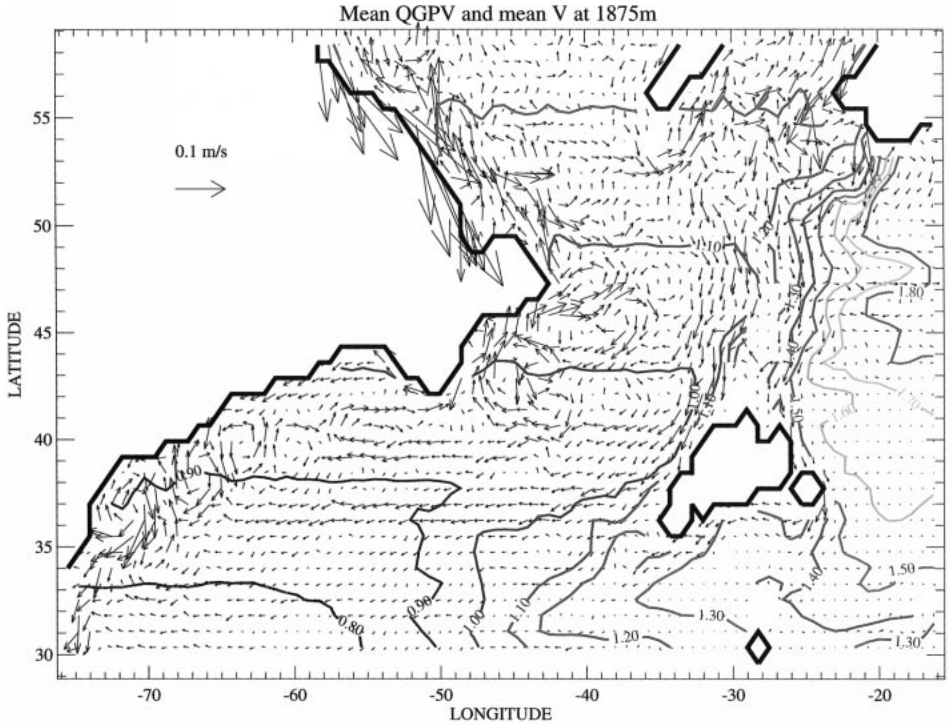

FIG. 15. Same as in Fig. 2 but for the 1875-m level. Contour interval for $\overline{q}$ is 0.1.

hypothesis does not explain the vertical homogenization of PV observed in Lozier's (1997) calculation and $\overline{P}$ calculated from the model output. In the pool of nearly homogenized $\overline{P}$ shown here, potential temperature and salinity are not nearly homogenized. We speculate that the vertical homogenization of $\overline{P}$ is simply an imported signal from the sinking region where a very deep column of small PV is created. As the water of small PV moves southward, the thickness of the low-PV water is modified due to near conservation of PV and mixing with the surrounding water.

To examine the pattern and strength of transport and mixing associated with the pool of nearly homogenized $\overline{P}$ or the pool of weakly varying $\overline{q}$, we calculated trajectories of 100 particles released from 15 different 2° × 2° areas. The particles are uniformly spread within the area of release at the beginning. The sites of particle release were chosen to cover the pool of nearly ho-

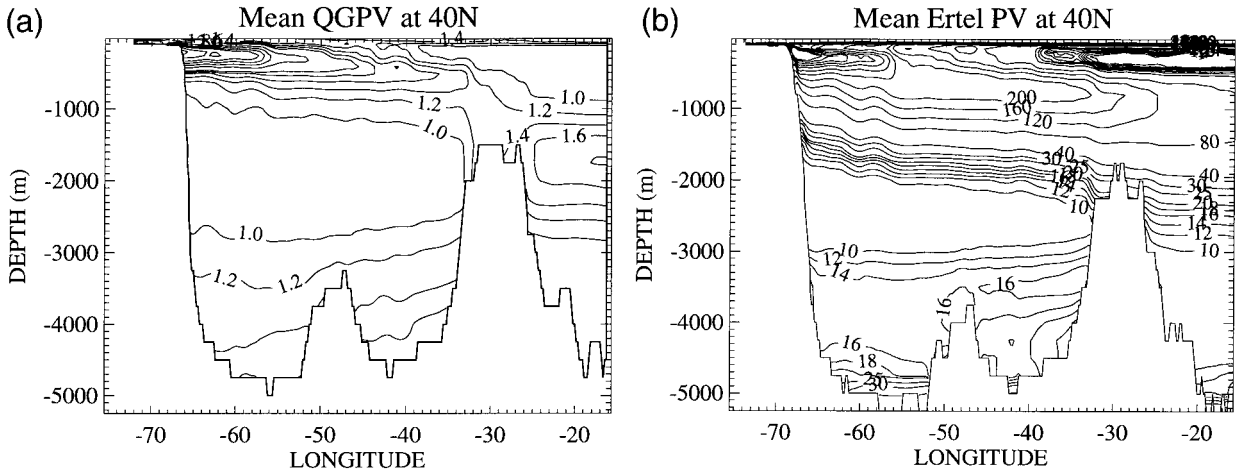

FIG. 16. Vertical cross sections of (a) $\overline{q}$ and (b) $\overline{P}$ at 40°N. Units for $\overline{q}$ and $\overline{P}$ are, respectively, 1×10^{-4} s^{-1} and 1×10^{-12} m^{-1} s^{-1}. Contours values are (a) 0.8, 1.0, 1.2, 1.4, 1.6, 1.8, 2.0, 2.5, 3.0, 3.5, 4.0, and 5.0; and (b) 10, 12, 14, 16, 18, 20, 25, 30, 40, 80, 120, 160, 200, 240, 280, 320, 360, 400, 440, and 480.

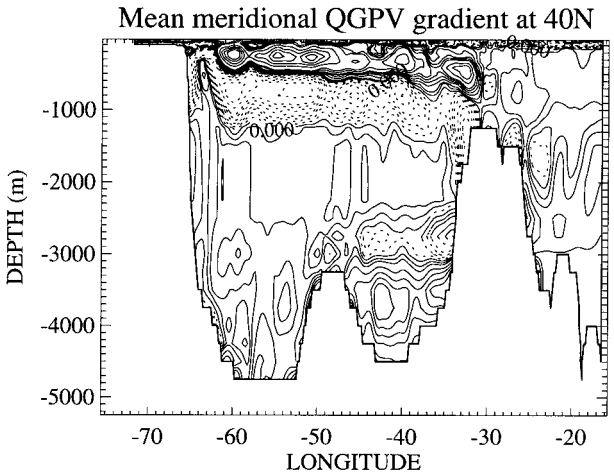

FIG. 17. Vertical cross section of $\partial\overline{q}/\partial y$ at 40°N. Units are 1×10^{-4} s^{-1} (100 km)$^{-1}$.

TABLE 2. Trajectory calculation initial particle release area number, release site location, flow used for particle advection, and the mean trajectory length of 100 particles. The release location is indicated by longitudinal and meridional extent in degrees. The mean trajectory length is given in kilometers. The flow used for these cases is from the model's 1875-m level. See text for details.

Area	Initial position		Flow type	Mean pathlength
	Lat (°N)	Long (°W)		
1	35–37	68–70	Full	18 075
1	35–37	68–70	Mean	6310
2	35–37	58–60	Full	13 083
2	35–37	58–60	Mean	5336
3	39–41	58–60	Full	16 438
3	39–41	58–60	Mean	3736
4	35–37	48–50	Full	8355
4	35–37	48–50	Mean	2933
5	39–41	48–50	Full	15 068
5	39–41	48–50	Mean	5886
6	35–37	38–40	Full	9861
6	35–37	38–40	Mean	2354
7	39–41	38–40	Full	13 593
7	39–41	38–40	Mean	5604
8	45–47	38–40	Full	15 491
8	45–47	38–40	Mean	7336
9	50–52	38–40	Full	12 986
9	50–52	38–40	Mean	5960
10	54–56	38–40	Full	10 559
10	54–56	38–40	Mean	3150
11	39–41	33–35	Full	12 293
11	39–41	33–35	Mean	4577
12	48–50	33–35	Full	13 791
12	48–50	33–35	Mean	4606
13	52–54	33–35	Full	12 405
13	52–54	33–35	Mean	6225
14	43–45	28–30	Full	8853
14	43–45	28–30	Mean	3220
15	48–50	28–30	Full	12 680
15	48–50	28–30	Mean	5495

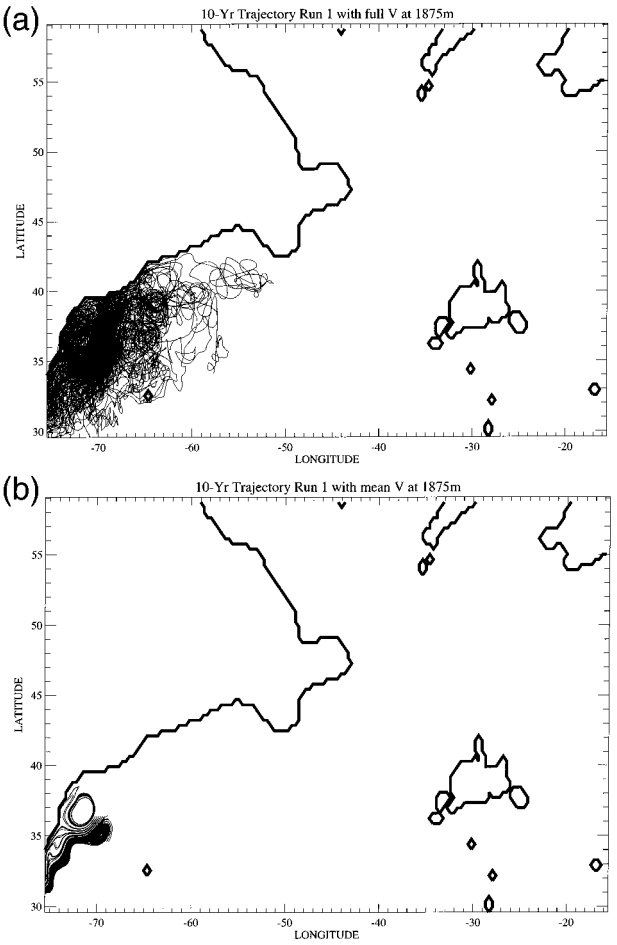

FIG. 18. Trajectories of 100 particles released from a 2° × 2° area covering 35°–37°N, 70°–68°W (area 1). The particles are evenly spaced at the beginning and then advected by (a) the full flow or (b) the mean flow at 1875 m for 10 years.

mogenized $\overline{P}$ at the $\overline{\sigma}_{2125\text{m}} = 37.5$ level or the pool of weakly varying $\overline{q}$ at 1875 m. For each initial particle release site, we ran a pair of 10-yr trajectory calculations; one with the full flow and the other with the mean flow. At these levels, the flow is considerably weaker than it is in the thermocline. To obtain a clearer picture of the pattern of transport and mixing, we chose to extend the trajectory run by repeating the 5-yr flow time series twice for the full-flow calculations. Since we are concerned with the overall pattern of transport and mixing and not the exact paths of individual particles, we believe that repeating the flow time series does not affect the results. The 15 areas of particle release and the mean trajectory length for each run are given in Table 2.

Five pairs of the 15 runs are shown as representative examples in Figs. 18–22. The areas of particle release for the runs shown in Figs. 18–22 are, in the same order, area 1, area 5, area 6, area 9, and area 12. Area 1 is located near the southwestern edge of the pool of nearly homogenized $\overline{P}$ just to the east of the center of a sta-

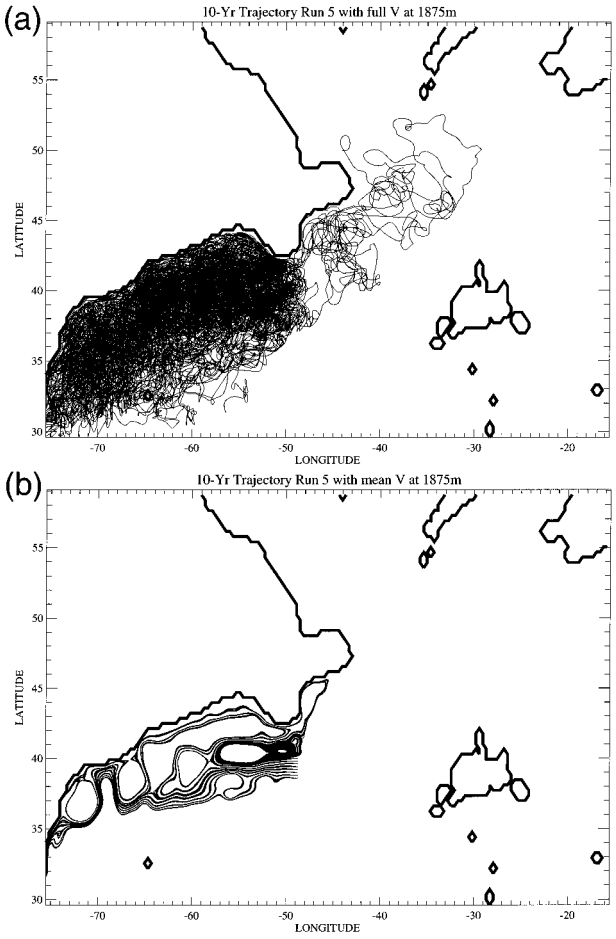

FIG. 19. Same as in Fig. 18 but for particles that are released from a 2° × 2° area covering 39°–41°N, 50°–48°W (area 5).

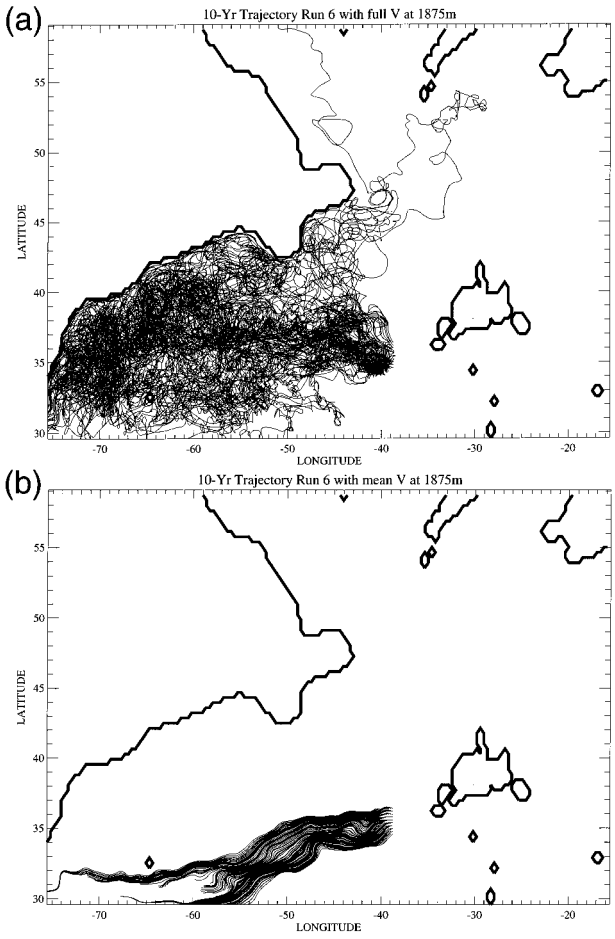

FIG. 20. Same as in Fig. 18 but for particles that are released from a 2° × 2° area covering 35°–37°N, 40°–38°W (area 6).

tionary anticyclonic eddy where the southward mean flow is very strong. Reflecting the southward mean flow, most of the particles are rapidly advected out the pool (Fig. 18). Eddy mixing does, however, spread some particles back into the pool against the mean flow advection (compare Figs. 18a and 18b). Area 5 is located near the center of the pool of nearly homogenized $\overline{P}$ or weakly varying $\overline{q}$. Particles released from area 5 are mostly trapped in the western half of the pool through the end of the run, while some exit the pool near the western boundary (Fig. 19). Although the spread of the particles is much weaker when the mean flow is used for advection, the trajectories calculated with the mean flow outline the area of particle spread calculated with the full flow (compare Figs. 19a and 19b). In general, particles released near the southern or eastern rim of the pool are advected out of the pool without recirculating back into the pool when only the mean flow is used (Fig. 20b). The Effect of eddy transport is to spread the particles into the pool, allowing many to remain in the pool through the end of the run (compare Figs. 20a and 20b), thereby increasing the residence time of particles within the pool. The effect of eddy transport becomes more conspicuous when the particles are released farther upstream near the rim. In fact, when the particles are released from outside the pool of nearly homogenized $\overline{P}$ but within the pool of weakly varying $\overline{q}$, many particles are transported northward by eddies and spread widely in the pool of nearly homogenized $\overline{P}$ or weakly varying $\overline{q}$ and tend to ''spread over'' the entire pool of weakly varying $\overline{q}$. This pattern of eddy mixing of particles from the rim or just outside the rim of the pool into the pool indicates (in terms of P) downgradient mixing or diffusion of P. When particles are released in the northern part of the pool, they tend to ''spread over'' the entire pool with the full flow advection (Fig. 21a). With the mean flow advection, they tend to outline the rim of the pool (Fig. 21b), with some particles recirculating in a small gyre occupying the northern half of the pool. Again, the strong effect of eddies in spreading the particles is clear. When the particles are released inside a small gyre in the northern half of the pool, they are completely trapped when the mean flow is used, while they are spread in the entire pool

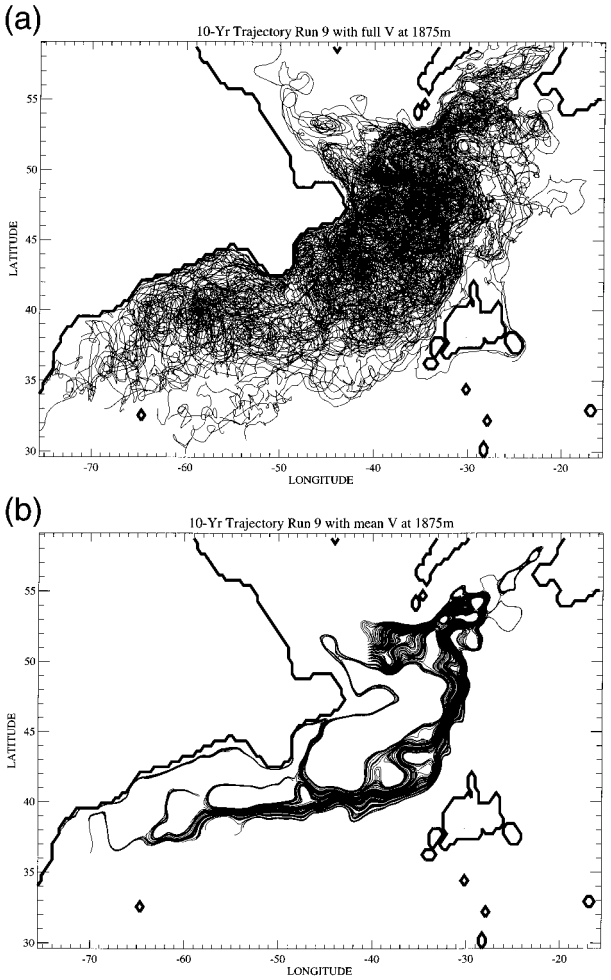

FIG. 21. Same as in Fig. 18 but for particles that are released from a 2° × 2° area covering 50°–52°N, 40°–38°W (area 9).

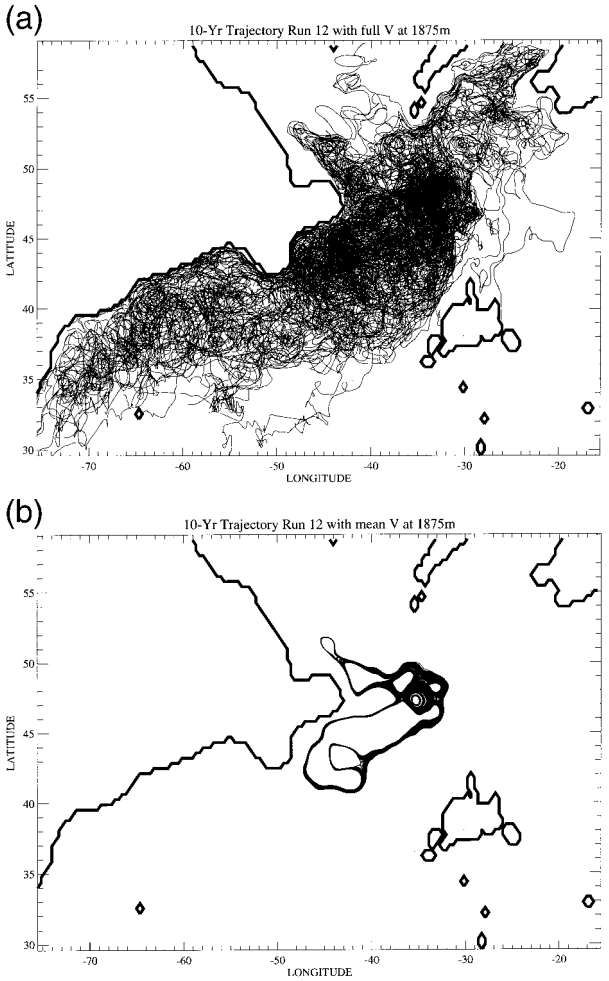

FIG. 22. Same as in Fig. 18 but for particles that are released from a 2° × 2° area covering 48°–50°N, 35°–33°W (area 12).

with the full-flow advection (Fig. 22). This is an extreme case that exemplifies the effect of eddy mixing. As in the calculations done with 577-m flows, we calculated the average trajectory pathlength of a particle for each run as a crude indicator of advection strength. The averages for all 15 runs with the full flow and the mean flow are, respectively, 12 902 km and 4849 km. The ratio of the two is 2.7. As in the case for the thermocline, the ratio suggests that the contribution of eddy advection is almost twice greater than that of the mean flow advection.

As shown in these example cases, particles released within or just outside of the pool of nearly homogenized $\overline{P}$ or weakly varying $\overline{q}$ are spread widely within the pool. When the mean flow is used, none of the 15 cases shows a complete recirculating gyre that encircles the pool of nearly homogenized $\overline{P}$, although many particles show a smaller recirculation in the northern half of the pool (Figs. 21 and 22). While the observation suggests the presence of a large recirculating gyre in the mean flow near the rim of the pool (Lozier 1997), the model shows only a smaller recirculation. This is likely to be related to the lack of an organized deep GS in the model, which is probably connected to unrealistically strong quasi-stationary eddies just downstream of the separation point. The lack of a deep GS in the model suggests that the model underestimates the mean flow advection and its impact on the structures of $\overline{P}$ and $\overline{q}$. However, the model considerably underestimates the eddy kinetic energy also. Thus, we believe that the effect of eddy mixing in the real ocean is strong, as suggested in the current study. The pool of nearly homogenized $\overline{P}$ resembles that predicted by the theory of Rhines and Young (1982a,1982b). The strong eddy mixing observed here does not conflict with the requirement of small $\nabla \cdot \overline{\mathbf{V}'P'}$, since $\overline{\mathbf{V}'P'} \approx 0$ within a pool of homogenized $\overline{P}$ no matter how strong the eddy motion. The eddy motion needs to be weak only near the rim of the pool where the gradient in $\overline{P}$ is finite. An intriguing point to note is the presence of an apparent mixing barrier along the MAR. Even when the trajectory calculations were extended for another 10 yr, few particles

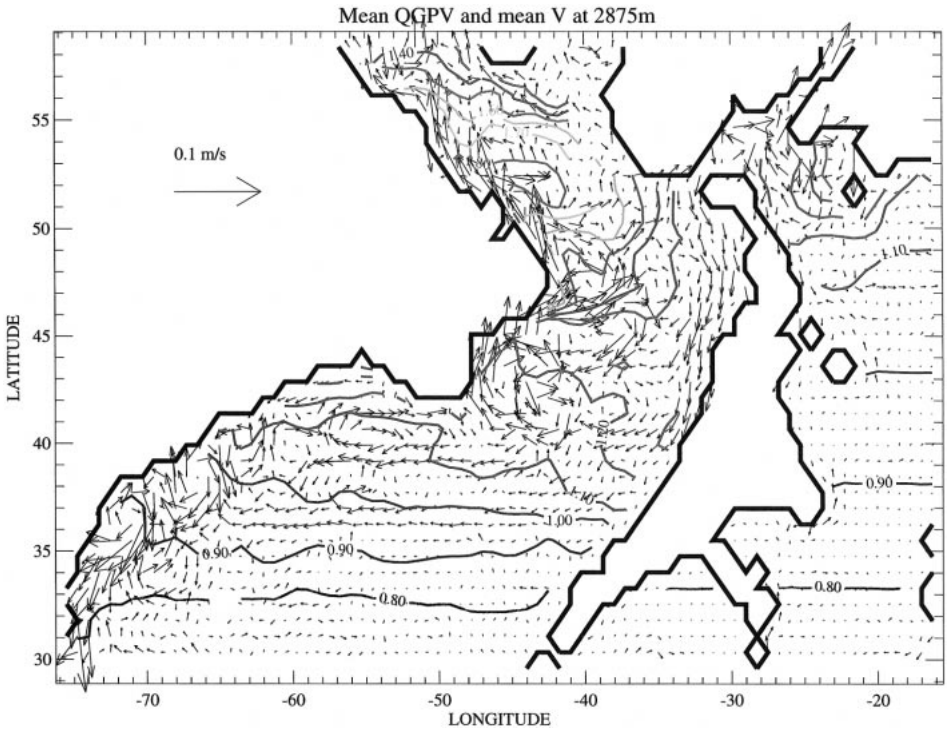

FIG. 23. Same as in Fig. 2 but for 2875-m level. The contour interval for $\overline{q}$ is 0.1.

penetrate to the east of the MAR. From the pattern of mixing and the structure of $\overline{P}$ shown here, we speculate the following picture. Low-P water is created in the sinking region by intense surface cooling and is advected southward toward the eastern rim of the pool of nearly homogenized $\overline{P}$. As the low-P water moves southward, it is mixed with waters of relatively high P, originating from the eastern side of the MAR, and with waters that have been circulating within the pool. After the water is mixed in the pool and circulates for some time, it exits the pool at the western end of the pool just off the western boundary. As Lozier (1997) pointed out, if such a circulation pattern indeed exists, it could have a substantial impact on the tracer ages and, more importantly, on climate signals originating in the sinking region. It also plays an important role in the stability characteristics of the GS.

Finally, we note that the flow (both the time-mean and eddy) to the east of the MAR is much weaker than that on the western side. This fact, together with the tight $\overline{q}$ and $\overline{P}$ contours seen in the region, suggests considerably weaker mixing to the east of the MAR. A small number of calculations for trajectories of particles released from areas to the east of the MAR show weak mixing (not shown), in agreement with the weak flow and tight $\overline{q}$ contours there.

4) DEEP WATERS

Below the 2375-m level, the characteristics of $\overline{q}$ change significantly again. Figure 23 shows $\overline{q}$ at 2875 m. At these deep levels, the stretching term becomes large again to the west of the MAR and stronger gradients in $\overline{q}$ are maintained. On the other hand, to the east of the MAR, the effect of the Mediterranean Overflow disappears and $\overline{q}$ is dominated by f. Trajectory calculations show that mixing at these levels is significantly weaker than the strong mixing in the layer of weakly varying $\overline{q}$ above, to the west of the MAR, suggesting that strength of mixing is an important factor in determining the structure of $\overline{q}$. The presence of finite meridional gradient in $\overline{q}$ at these levels is seen in the vertical cross sections as well (Fig. 16) and also is in agreement with the theory of baroclinic neutrality by Lindzen (1993) and idealized models of the wind-driven circulation (e.g., Holland et al. 1984). It is premature to conclude that the structure of $\overline{q}$ to the west of the MAR is indeed created by the baroclinic ocean's tendency toward baroclinic neutrality. Nevertheless, transient wave activity shows large values in the top 1000 m and below 2500 m with low values in the middle in this region (Nakamura and Chao 2000), supporting this hypothesis.

c. Eddy mixing indicators

In the preceding, we repeatedly refered to strong eddy mixing occuring in the model based on trajectory analyses. A more quantitative measure of the eddy mixing strength is K_e/K_m, where K_e and K_m are, respectively, the eddy and mean kinetic energy. Holland and Rhines

(1980) and Rhines and Schopp (1991) calculated K_e/K_m from output of an idealized eddy-resolving model and found that the values are typically 1 to 10 in upper layers and 10 or greater in the mid to lower layers, suggesting stronger eddy mixing (with respect to the mean) in the mid to lower layers. We have found qualitatively the same result in this more realistic model output. Figure 24 shows K_e/K_m at 6 and 577 m. At 6 m, the values are less than 10 in most of the domain. Below the top 50 m or so, the values are greater than 10 in a large portion of the domain. These large values in K_e/K_m are in agreement with the strong eddy mixing indicated by trajectory calculations.

Another quantitative indicator for eddy mixing is the Peclet number, Pe. To estimate Pe from the model output, we adopted the formula derived by Rhines and Schopp (1991). The formula is $|\overline{\mathbf{V}} \times \nabla\overline{q}|/|\overline{\mathbf{V}} \cdot \nabla\overline{q}|$. Rhines and Schopp (1991) note that the formula is valid at levels where diabatic forcing of q is weak. We computed Pe with this formula below 200 m in the model. Figure 25 shows Pe at 233 m. The figure is shown as a typical example of Pe at all levels. In general, the field is very noisy with many small areas of large Pe due to the division by $|\overline{\mathbf{V}} \cdot \nabla\overline{q}|$ in the formula. The very large values appear random, suggesting that they are most likely noise. The only exception is just off the western boundary north of 50°N, where a very stable boundary current flows southward and shows very weak eddy activity. At almost all levels, Pe is less than 5 in 60% of the total area and less than 10 in 80% of the total area. These moderate values of Pe are in agreement with the estimate for the eastern North Atlantic given by Dickson (1989) and values calculated from idealized model output by Rhines and Schopp (1991), and suggest strong eddy mixing in the model as indicated by particle trajectories.

5. Summary

We have examined the output of an eddy-resolving GCM of the North Atlantic in a framework based on quasigeostrophic potential vorticity, q, to study the large-scale circulation in the model ocean. The model q field is dominated by the planetary vorticity and the stretching term everywhere most of the time. Near the surface, above 150 m, the evolution of q field reflects strong seasonal effect of the diabatic heating and cooling on the stretching term. The seasonal effect is particularly pronounced in the shallow regions to the north of the GS. Between 150 and 1000 m, the q field evolution is characterized by vigorous q input by the GS and mixing of high-q fluid with the surrounding along the path of the GS. Strong mixing of fluid associated with growth, breaking, and decay of waves in the vicinity of the GS is clearly seen at these levels. In the time mean, the input of q by the GS and wave-induced mixing along its path result in a broad tonguelike structure of high $\overline{q}$ along the path of the GS. This tongue of high $\overline{q}$ shifts southward with depth until it disappears at around 1000 m. There are qualitative similarities between horizontal $\overline{q}$ structures at these levels and isopycnal structures of PV at levels in the same range computed by Keffer (1985) from the Levitus dataset. Between 1000 and 2500 m, q field characteristics are completely different from those at upper levels. Large values are seen to the east of the Mid-Atlantic Ridge (MAR) due to the Mediterranean overflow. The high-q fluid originates from the northeastern corner of the domain studied here and gradually spreads southward. Fluid in this region shows only weak motion. To the west of the MAR at these levels, q is essentially equal to the planetary vorticity and is mixed vigorously by wavelike motions. The time-mean pictures reflect these features of q and show very weak structures with small values of $\overline{q}$ to the west of the MAR and relatively large values of $\overline{q}$ increasing toward the northeast to the east of the MAR. There are qualitative similarities in the horizontal structure between $\overline{q}$ at these levels and PV at levels in the same range computed from an improved hydrographic dataset by Lozier (1997). Below 2500 m to the bottom, q field evolution is weak on both sides of the MAR, but that to the west of the MAR shows substantially stronger wavelike motions than that to the east of the MAR. At these deep levels, q and $\overline{q}$ show nonnegligible contribution of the stretching term to the west of the MAR again, while they are essentially equal to the planetary vorticity to the east of the MAR.

The 3D structure of $\overline{P}$ calculated from the mean potential temperature and salinity in the model to the west of the MAR, particularly where the influence of the GS is observed, shows an interesting qualitative similarity to that of the midlatitude atmosphere. It is characterized by large positive meridional gradient near the surface, nearly homogenized $\overline{P}$ from, approximately, 2000 to 3000 m, and again relatively large meridional gradient near the bottom. Near the top of the pool of nearly homogenized $\overline{P}$, there is a layer of small negative meridional gradient of $\overline{P}$, suggesting that active baroclinic waves are supported in the region. The 3D structure of $\overline{q}$ also supports the presence of active baroclinic waves in the region. Lindzen (1993) argues that such a structure of PV may be a consequence of baroclinic flow's tendency toward the baroclinic neutrality. Crude estimates of the depth of the pool of the nearly homogenized $\overline{P}$ or weak gradients in $\overline{q}$ based on the theory are within a reasonable range, supporting the hypothesis.

In the model used here, advection and mixing by eddies are found to be strong in general. The ratio of the eddy kinetic energy to the mean kinetic energy, Peclet number, and trajectory analyses all suggest an important role of eddies in mixing and advection and, thus, shaping of the $\overline{P}$ and $\overline{q}$ fields. Also, a clear sign of directional dependence in the mixing pattern is observed in trajectory analyses, suggesting the need for eddy mixing parameterizations that reflect the dependence in coarse-resolution models.

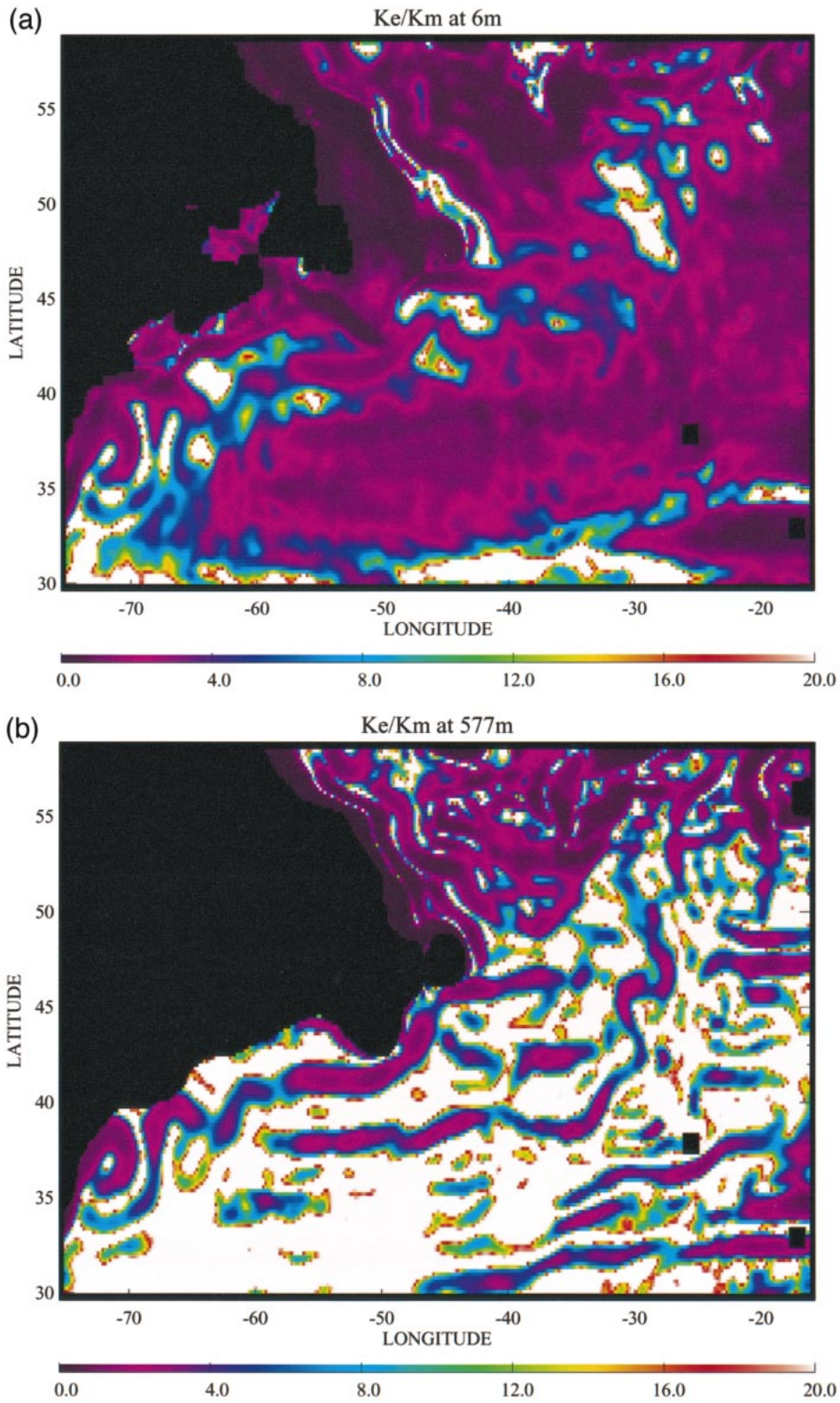

FIG. 24. Color plot of K_e/K_m at (a) 6 m and (b) 577 m, where K_e and K_m are, respectively, eddy kinetic energy and mean kinetic energy.

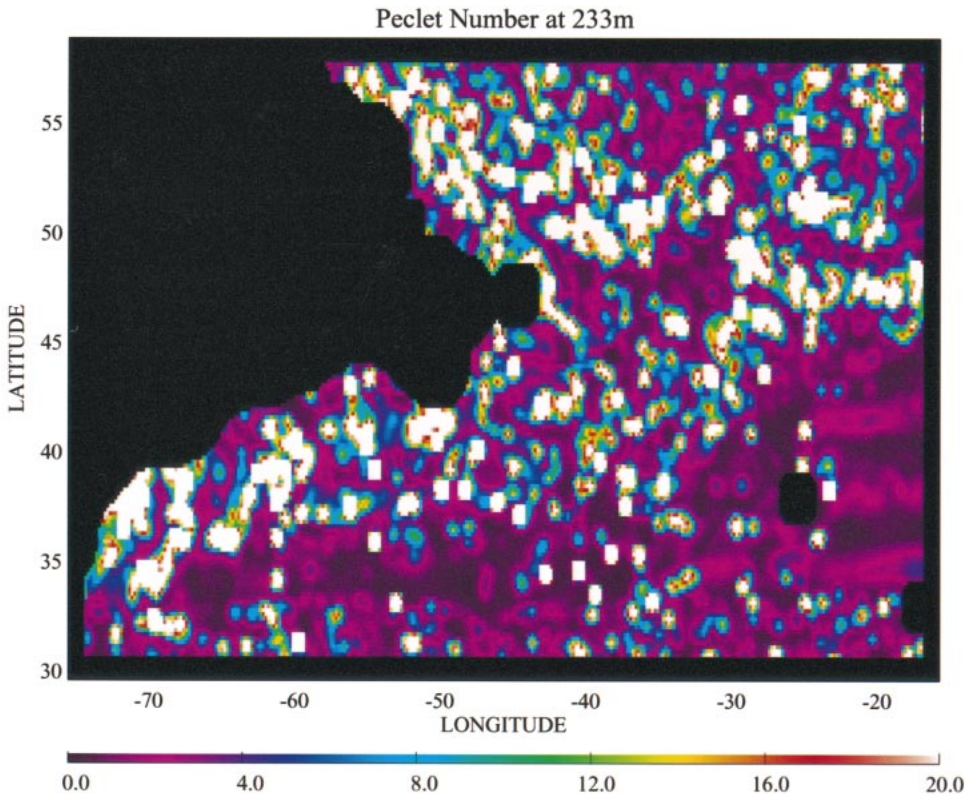

FIG. 25. Color plot of Peclet number at 233 m.

In the absence of sufficient data to study dynamics and kinematics of the real oceanic flows on a basin scale or larger, development of realistic ocean models that can supply pseudo data is crucial, as well as improvement in data measurement that can supply oceanic data to constrain such models. In this paper, we have attempted to demonstrate the potential usefulness of pseudo data in studying large-scale oceanic circulations. We emphasize that the time mean of the pseudodata used here, model output from the 25th to 29th year of an integration, is representative of a low-frequency state of the model ocean in these years. The model deep waters are almost certainly not in equilibrium, implying that the upper levels are probably not in equilibrium either due to the impact of deep PV structures on upper-level flows. Therefore, the model flow is likely to have not reached statistical steady state either. The reader should be aware of this limitation and consider the present results as a low-frequency state analyses of an evolving model flow. Due to the limitation on the computational resources, running the model for several hundred years until it reaches a statistical steady state is not feasible for us. Diagnoses of eddy potential enstrophy and eddy fluxes of q using the same model output is reported in a companion paper, NC. Extensive measurement of oceanic properties at intervals sufficient to resolve the important eddies is not likely to materialize in the foreseeable future. In light of this limitation in the data availability, cautious use of eddy-resolving model output may be of substantial merit in studying large-scale oceanic circulations.

Acknowledgments. The research described in this paper was carried out by the Jet Propulsion Laboratory (JPL), California Institute of Technology, under contract with National Aeronautics and Space Administration. Computations were carried out on the 256-processor Cray T3D through the JPL Supercomputing Project. Nakamura is indebted to John Marshall for stimulating conversations that led to this series of diagnoses. We are grateful to Susan Lozier for helpful communication and Mike Spall for helpful comments on the draft of the paper. Finally, we wish to thank Meghan Cronin and an anonymous reviewer for helpful comments and suggestions on the manuscript.

REFERENCES

Beckman, A., C. W. Böning, C. Köberle, and J. Willebrand, 1994: Effects of increased horizontal resolution in a simulation of the North Atlantic Ocean. *J. Phys. Oceanogr.*, **24,** 326–344.

Behringer, D. W., 1972: Investigations of large scale oceanic circulation patterns using historical hydrographic data. Ph.D. thesis, University of California, San Diego.

Böning, C. W., and M. D. Cox, 1988: Particle dispersion and mixing of conservative properties in an eddy-resolving model. *J. Phys. Oceanogr.,* **18,** 320–338.

Bryan, F. O., and W. R. Holland, 1989: A high resolution simulation of the wind- and thermohaline-driven circulation in the North Atlantic Ocean. *'Aha Huliko'a Parameterization of Small-Scale Processes,* P. Müller and D. Henderson, Eds., Hawaii Institute of Geophysics, 99–115.

Bryan, K., 1969: A numerical method for the study of the circulation of the World ocean. *J. Comput. Phys.,* **4,** 347–376.

Carton, J., and Y. Chao, 1999: Caribbean Sea eddies inferred from TOPEX/Poseidon altimetry and an eddy-resolving Atlantic Ocean model. *J. Geophys. Res.,* **104,** 7743–7752.

Cayan, D. R., 1992a: Latent and sensible heat flux anomalies over the northern oceans: The connection to monthly atmospheric circulation. *J. Climate,* **5,** 354–369.

——, 1992b: Latent and sensible heat flux anomalies over the northern oceans: Driving the sea surface temperature. *J. Climate,* **5,** 859–881.

Chao, Y., A. Gangopadhyay, F. O. Bryan, and W. R. Holland, 1996: Modeling the Gulf Stream: How far from reality? *Geophys. Res. Lett.,* **23,** 3155–3158.

Charney, J. G., and M. E. Stern, 1962: On the instability of internal baroclinic jets in a rotating atmosphere. *J. Atmos. Sci.,* **19,** 159–172.

Cox, M. D., 1984: A primitive equation, 3-dimensional model of the ocean. GFDL Ocean Group Tech. Rep. No. 1, GFDL/Princeton University.

——, 1985: An eddy resolving numerical model of the ventilated thermocline. *J. Phys. Oceanogr.,* **15,** 1312–1324.

Dickson, R. R., 1989: Flow statistics from long-term current-meter moorings: The global dataset in January 1989. World Climate Program Rep. WCRP-30, WMO.

Dukowicz, J. K., and R. D. Smith, 1994: Implicit free-surface method for the Bryan-Cox-Semtner ocean model. *J. Geophys. Res.,* **99,** 7991–8014.

Eady, E. T., 1949: Long waves and cyclone waves. *Tellus,* **1,** 33–52.

Ferranti, L., F. Molteni, and T. N. Palmer, 1994: Impact of localized tropical and extratropical SST anomalies in ensembles of seasonal GCM integrations. *Quart. J. Roy. Meteor. Soc.,* **120,** 1613–1645.

Gill, A. E., 1982: *Atmosphere–Ocean Dynamics.* Academic Press, 662 pp.

Halliwell, G. R., Jr., and C. N. K. Mooers, 1983: Meanders of the Gulf Stream from Cape Hatteras 1975–1978. *J. Phys. Oceanogr.,* **13,** 1275–1292.

Holland, W. R., 1978: The role of mesoscale eddies in the general circulation of the ocean—Numerical experiments using a wind-driven quasi-geostrophic model. *J. Phys. Oceanogr.,* **8,** 363–392.

——, and P. B. Rhines, 1980: An example of eddy-induced ocean circulation. *J. Phys. Oceanogr.,* **10,** 1010–1031.

——, T. Keffer, and P. B. Rhines, 1984: Dynamics of the oceanic general circulation: The potential vorticity field. *Nature,* **308,** 698–705.

Hoskins, B. J., and P. D. Sardeshmukh, 1987: A diagnostic study of the dynamics of the Northern Hemisphere winter of 1985–86. *Quart. J. Roy. Meteor. Soc.,* **113,** 759–778.

——, and P. J. Valdes, 1990: On the existence of storm-tracks. *J. Atmos. Sci.,* **47,** 1854–1864.

——, M. E. McIntyre, and A. W. Robertson, 1985: On the use and significance of isentropic potential vorticity maps. *Quart. J. Roy. Meteor. Soc.,* **111,** 877–946.

Hurrell, J. W., and H. van Loon, 1997: Decadal variations in climate associated with the North Atlantic Oscillation. *Climatic Change,* **36,** 301–326.

Illari, L., and J. C. Marshall, 1983: On the interpretation of eddy fluxes during a blocking episode. *J. Atmos. Sci.,* **40,** 2232–2242.

Keffer, T., 1985: The ventilation of the world's oceans: Maps of the potential vorticity field. *J. Phys. Oceanogr.,* **15,** 509–523.

Levitus, S., 1982: *Climatological Atlas of the World Ocean.* NOAA Prof. Paper No. 13, U.S. Govt. Printing Office, Washington, DC, 173 pp.

——, R. Burgett, and T. P. Boyer, 1994: *World Ocean Atlas 1994.* Vol. 3: *Salinity.* NOAA Atlas NESDIS 3, U.S. Dept. of Commerce, 99 pp.

Lindzen, R. S., 1993: Baroclinic neutrality and the tropopause. *J. Atmos. Sci.,* **50,** 1148–1151.

Lozier, M. S., 1997: Evidence for large-scale eddy-driven gyres in the North Atlantic. *Science,* **277,** 361–354.

——, 1999: The impact of mid-depth recirculations on the distribution of tracers in the North Atlantic. *Geophys. Res. Lett.,* **26,** 219–222.

——, and S. C. Riser, 1989: Potential vorticity dynamics of boundary currents in a quasi-geostrophic ocean. *J. Phys. Oceanogr.,* **19,** 1373–1396.

——, and ——, 1990: Potential vorticity sources and sinks in quasi-geostrophic ocean: Beyond western boundary currents. *J. Phys. Oceanogr.,* **20,** 1608–1627.

——, W. B. Owens, and R. G. Curry, 1995: The climatology of the North Atlantic. *Progress in Oceanography,* Vol. 36, Pergamon, 1–44.

McDowell, S., P. B. Rhines, and T. Keffer, 1982: North Atlantic potential vorticity and its relation to the general circulation. *J. Phys. Oceanogr.,* **12,** 1417–1436.

Nakamura, M., and Y. Chao, 2000: Characteristics of three-dimensional quasi-geostrophic transient eddy propagation in the vicinity of a simulated Gulf Stream. *J. Geophys. Res.,* **105,** 11 385–11 406.

Owens, W. B., 1991: A statistical description of the mean circulation and eddy variability in the northwestern Atlantic using SOFAR floats. *Progress in Oceanography,* Vol. 28, Pergamon, 257–303.

Palmer, T. N., and Z. Sun, 1985: A modelling and observational study of the relationship between sea surface temperatures in the northwest Atlantic and the atmosphere general circulation. *Quart. J. Roy. Meteor. Soc.,* **111,** 947–975.

Pauluhn, A., and Y. Chao, 1999: Tracking eddies in the subtropical north-western Atlantic Ocean. *Phys. Chem. Earth,* **24A,** 415–421.

Phillips, N. A., 1954: Energy transformation and meridional circulations associated with simple baroclinic waves in a two-level quasi-geostrophic model. *Tellus,* **6,** 273–286.

Rhines, P. B., and W. R. Holland, 1979: A theoretical discussion of eddy-driven mean flows. *Dyn. Atmos. Oceans,* **3,** 289–325.

——, and W. R. Young, 1982a: A theory of wind-driven ocean circulation. I: Mid-ocean gyres. *J. Mar. Res.,* **40** (Suppl.), 559–596.

——, and ——, 1982b: Homogenization of potential vorticity in planetary gyres. *J. Fluid Mech.,* **122,** 347–368.

——, and R. Schopp, 1991: The wind-driven circulation: Quasi-geostrophic simulations and theory for nonsymmetric winds. *J. Phys. Oceanogr.,* **21,** 1438–1469.

Richardson, P. L., 1993: A census of eddies observed in North Atlantic SOFAR float data. *Progress in Oceanography,* Vol. 31, Pergamon, 1–50.

Schmitz, W. J., and J. D. Thompson, 1993: On the effects of horizontal resolution in a limited-area model of the Gulf Stream system. *J. Phys. Oceanogr.,* **23,** 1001–1007.

Semtner, A. J., and R. M. Chervin, 1992: Ocean general circulation from a global eddy-resolving model. *J. Geophys. Res.,* **97,** 5493–5550.

Smith, R. D., J. K. Dukowicz, and R. C. Malone, 1992: Parallel ocean general circulation modeling. *Physica D,* **60,** 38–61.

Spall, M. A., 1996: Dynamics of the Gulf Stream/deep western boundary current crossover. Part I: Entrainment and recirculation. *J. Phys. Oceanogr.*, **26,** 2152–2168.

Stone, P. H., 1978: Baroclinic adjustment. *J. Atmos. Sci.*, **35,** 561–571.

Tracey, K. L., and D. R. Watts, 1986: On Gulf Stream meander characteristics near Cape Hatteras. *J. Geophys. Res.*, **91,** 7587–7602.

Wallace, J. M., C. Smith, and Q. Jiang, 1990: Spatial patterns of atmosphere–ocean interaction in the northern winter. *J. Climate*, **3,** 990–998.

Watts, D. R., K. L. Tracey, J. M. Bane, and T. J. Shay, 1995: Gulf Stream path and thermocline structure near 74°W and 68°W. *J. Geophys. Res.*, **100,** 18 291–18 312.

Worthington, L. V., 1959: The 18° Water in the Sargasso Sea. *Deep-Sea Res.*, **5,** 205–211.